



City Research Online

City, University of London Institutional Repository

Citation: Georgoulas, A., Koukouvinis, P., Gavaises, M. & Marengo, M. (2015). Numerical investigation of quasi-static bubble growth and detachment from submerged orifices in isothermal liquid pools: The effect of varying fluid properties and gravity levels. *International Journal of Multiphase Flow*, 74, pp. 59-78. doi: 10.1016/j.ijmultiphaseflow.2015.04.008

This is the accepted version of the paper.

This version of the publication may differ from the final published version.

Permanent repository link: <https://openaccess.city.ac.uk/id/eprint/13578/>

Link to published version: <https://doi.org/10.1016/j.ijmultiphaseflow.2015.04.008>

Copyright: City Research Online aims to make research outputs of City, University of London available to a wider audience. Copyright and Moral Rights remain with the author(s) and/or copyright holders. URLs from City Research Online may be freely distributed and linked to.

Reuse: Copies of full items can be used for personal research or study, educational, or not-for-profit purposes without prior permission or charge. Provided that the authors, title and full bibliographic details are credited, a hyperlink and/or URL is given for the original metadata page and the content is not changed in any way.

City Research Online:

<http://openaccess.city.ac.uk/>

publications@city.ac.uk

Numerical investigation of quasi-static bubble growth and detachment from submerged orifices in isothermal liquid pools: The effect of varying fluid properties and gravity levels

A. Georgoulas^{a,b,*}, P. Koukouvinis^{c,d}, M. Gavaises^c and M. Marengo^{a,e}

^aDepartment of Engineering, University of Bergamo, Viale Marconi 5, 24044 Dalmine (BG), Italy

^bEngine Research and Development Centre, Caterpillar Inc., Frank Perkins Parkway, PE1 5FQ Peterborough, UK

^cSchool of Engineering and Mathematical Sciences, City University London Northampton Square, London, EC1V 0HB

^dCaterpillar Fuel Systems (CFS), Mossville, Illinois, USA

^eSchool of Computing, Engineering and Mathematics, Cockcroft Building, Lewes Road, University of Brighton, Brighton, UK

* Corresponding author. Tel.: +390352052067. E-mail address: anastasios.georgoulas@unibg.it (A. Georgoulas).

ABSTRACT

The present investigation, identifies the exact quantitative effects of fundamental parameters, on the detachment characteristics of isolated bubbles, emanating quasi-statically from submerged orifices into isothermal liquid pools. For this purpose, a Volume of Fluid (VOF) based interface capturing approach is further improved, for the conduction of axisymmetric and 3D numerical experiments on adiabatic bubble growth dynamics. The predictions of the model, are quantitatively validated against literature available experimental data, showing excellent agreement. Two series of numerical experiments are performed, quantitatively exploring the parametric effects of the liquid phase properties in five different gravity levels, and the effect of the gravity vector direction inclination angle, respectively. It is found that the bubble detachment characteristics, are more sensitive in the variation of the surface tension, liquid phase density and gravity, while the effect of liquid phase dynamic viscosity is generally minimal. From dimensionless analysis, two correlations are derived, which for the examined range of Eötvös numbers, are able to predict the equivalent bubble detachment diameter and the bubble detachment time, respectively. It is also found that the bubble detachment characteristics, reduce significantly as the gravity vector direction gradually deviates from being parallel to the bubble injection orifice, following a non-linear decrease.

KEY WORDS: Two-phase flow, Numerical simulation, VOF method, Adiabatic bubble dynamics, Bubble detachment characteristics.

1. INTRODUCTION

The investigation of bubble growth and detachment has received a lot of attention over the last years, due to its occurrence in a wide range of domestic and industrial applications as well as because it is considered to be a fundamental process, for understanding more complicated phenomena such as boiling. Application examples include among others, heat exchangers, electronic cooling, chemical processing, emulsion preparation in boilers, beer production and waste water remediation. Also in space technology the bubble dynamics are important for cryocoolers and for two-phase thermal systems, like thermosyphons. However, there is still an incomplete understanding of the fundamental physics of bubble dynamics, at small scales as well as at non-trivial geometrical configurations. Therefore, the isolation and understanding of the influence of various fundamental controlling parameters individually, is necessary. In order to investigate bubble dynamics, an adiabatic/isothermal approach is often used, where gas/vapour bubbles are injected into liquid pools at isothermal/saturation conditions, from a submerged orifice. With such an approach, the bubble growth and detachment process can be carefully controlled, allowing thus the detailed quantitative investigation of the effect of fundamental controlling parameters.

During bubble formation at the tip of an orifice, the interaction between the gas/liquid or vapor/liquid phases is governed by a balance between aiding and restraining forces (Albadawi et al., 2013a; Di Bari and Robinson, 2013a; Di Bari et al., 2013). In more detail, the gas injection momentum, the pressure difference and the buoyancy forces are aiding the bubble growth and detachment process, while the inertia, viscous and surface tension forces tend to keep the bubble attached to the orifice. For the case of single bubble growth and detachment two different regimes have been identified (Benzing and Myers, 1955; Oguz and Prosperetti, 1993). In the first regime, where the gas injection flow rates are smaller than a critical value, the gas momentum and liquid inertia have much smaller influence compared to the surface tension and viscous forces. As a result, the buoyancy force is balanced mainly by surface tension and viscous effects, and the bubble detachment diameters are almost independent of gas flow rate in this regime. This regime is also known as quasi-static bubble growth regime (Di Bari et al., 2013; Gerlach et al., 2005). In contrast, beyond the critical gas flow rate (for a given orifice size), the effects of gas momentum, gas shear, pressure force, and liquid inertia are important. Therefore, in this second regime the bubble-departure diameter increases with respect to the flow rate, being also strongly dependent upon the orifice size (Subramani et al., 2007). Below a critical orifice size, the bubble detachment diameter increases with the corresponding increase of the orifice diameter, while an opposite behavior is observed for higher orifice diameters (Di Marco, 2005; Kasimsetty et al., 2007; Subramani et al., 2007). The present numerical investigation, focuses on the first regime of quasi-static bubble growth.

So far, many experimental, analytical and lately numerical works in the literature have been focused on the adiabatic gas/vapour injected bubble growth dynamics. In the early work of Davidson and Schüller (1960), an attempt is made to understand the phenomenon of bubble growth in both water and mineral oil, from various orifice diameters through experimental investigations. Later, several works have been focused in tracking the bubble shape and departure frequency for a variety of surrounding liquids (McCann and Prince, 1969; Swope, 1971; Walters and Davidson, 1962, 1963). The advancement of experimental measuring techniques the following decades, provided a great number of experimental works focusing on the adiabatic bubble growth and detachment characteristics, giving detailed insight regarding the influence of various controlling parameters such as orifice diameter, gas injection flow rate, surface tension, gas-liquid contact angles, viscosity and density ratios (Di Bari and Robinson, 2013b; Byakova et al., 2003; Tsuge et al., 2006; Zhang and Shoji, 2001; Zhu et al., 2010). Moreover, several researchers have also been focused in the process of adiabatic bubble formation and detachment under reduced gravity conditions (Chakraborty et al., 2009; Kim et al., 1994; Pamperin and Rath, 1995; Tsuge et al., 1997), identifying three distinct regimes during bubble growth in microgravity, the static, the dynamic and the turbulent regime. Finally, a considerable number of experimental works have been also focused in the effect of the presence of electric fields in the bubble growth and detachment characteristics (Di Bari and Robinson, 2013b; Di Marco et al., 2003).

All the above experimental efforts, have also generated a large number of different theoretical models that describe the process of adiabatic bubble growth and detachment from submerged orifices, based on different equations and laws. The early theoretical works on bubble growth were focused on the investigation of gas/liquid interfaces to predict the bubble behavior, assuming that the bubble maintains a spherical shape (Davidson and Schüller, 1960; Walters and Davidson, 1963). Oguz and Prosperetti (Oguz and Prosperetti, 1993) predicted the bubble volume, considering a force balance between buoyancy and surface tension, applying a Boundary Integral Method for the interface position. The Young–Laplace equation has also been applied for tracking the interface position during the process of bubble growth (Gerlach et al., 2005; Lee and Tien, 2009). However, the main limitation of the majority of these theoretical approaches is their inability to account for the viscous effects as well as the necking and pinch-off stages, before detachment.

Over the last decades, the continuous improvement in the available computational resources and the development of robust numerical methods, allowed the simulation of complex gas/liquid interface deformation in viscous fluid flows, by using

either the Eulerian interface capturing or the Lagrangian front tracking approaches. Both of these numerical techniques treat the two phases as a mixture, following a single fluid approach and solving a single set of Navier–Stokes equations typically on a fixed grid, with the mixture properties calculated in terms of the interface position. In front tracking methods (Unverdi and Tryggvason, 1992), the front is represented by a Lagrangian interface which is tracked using suitable adaptive marker elements, and advected using the flow field that is solved on a stationary mesh. Then, the details of the new position of the front are transferred to the fluid flow on the fixed grid, using a smooth distribution function. An extended version of this method (Hua and Lou, 2007), has been used for the study of bubble pinch-off, from a nozzle immersed in quiescent water by Quan and Hua (2008). On the other hand, with interface capturing methods, the interface is reconstructed from a volume fraction field which is advected by the fluid mixture velocity, on a fixed Eulerian grid. The most widely used interface capturing approaches are the Volume of Fluid (VOF) method and the Level Set (LS) method or a combination of these two, known as Combined Level Set and Volume of Fluid (CLSVOF) method. All these three methods, have been extensively developed and validated for a broad range of two-phase flows, including bubble flows. Worth mentioning examples on adiabatic bubble growth and detachment include the works of Gerlach et al. (2007), Pianet et al. (2010), Chakraborty et al. (2011), Albadawi et al. (2012), Albadawi et al. (2013a, 2013b), Di Bari et al. (2013). Other, different but quite promising numerical techniques for the investigation of bubble dynamics, that differ from the widely used, grid based CFD techniques of VOF, LS and CLSVOF, are the Smooth Particle Hydrodynamics (SPH) method (Das and Das, 2009, 2013) and the Lattice Boltzmann Method (LBM) (Frank et al., 2005).

It is worth mentioning that despite the large number of the experimental, analytical and numerical works so far, most of them deal with the formation, growth, and departure of spherical or non-spherical bubbles that follow a symmetric growth and detachment over the orifice mouth, using mainly water and air as the working fluids. In more detail, most of these works examine the effect of vapor injection mass flow rate and/or orifice geometrical characteristics and some works address the effects of surface tension, density and viscosity ratios as well as micro-gravity and/or hyper-gravity conditions but not in a comprehensive, quantitative manner. Furthermore, asymmetry in bubble shape during its growth and detachment is not uncommon, in real technological applications. Phase change induced bubble nucleation over inclined surfaces, can easily generate asymmetric bubble growth and detachment. Therefore, the numerical simulation of asymmetric bubble growth and detachment can provide valuable insight regarding the formation, sliding and detachment of bubbles over inclined surfaces.

Usually, the generated bubbles become asymmetric either when the orifice plane is inclined to the horizontal or under the influence of a cross flow. Gas/vapor bubble growth and detachment from an orifice mouth in a liquid cross flow is a quite common situation and it has already been investigated by various researchers throughout the years (Marshall et al., 1993; Forrester and Rielly, 1998), providing great insight regarding the shape evolution of the generated bubbles in different gas/liquid mass flow rates. However, the influence of orifice or orifice plate inclination on adiabatic bubble growth and detachment characteristics, has not yet been fully investigated. According to the authors' best knowledge, the only efforts in this direction are made by Kumar and Kuloor (1970), Das and Das (2013) and Di Marco et al. (2013). The understanding of the influence of orifice inclination on the bubble volume evolution as well as on its departure frequency can be considered to be essential. The orifice inclination is expected to alter significantly the hydrodynamics of the growing bubbles since the induced symmetry in vertical orifices is collapsed, rendering the whole growing process three-dimensional. Such problems cannot be handled by analytical solutions and even laboratory experiments and numerical simulations are difficult. In order to investigate in detail the bubble formation, growth, detachment or sliding over inclined surfaces and the quite complex hydrodynamics of the ambient liquid, 3-D numerical simulations are essential.

In the present investigation, the VOF based, interface capturing approach that is already implemented in OpenFOAM® CFD Toolbox (version 2.2.1), is accordingly modified in order to account for spurious currents reduction. At this point it should be mentioned that initial trial simulations with the original VOF based solver of OpenFOAM (interFoam), revealed that due to erroneous calculation of the interface curvature, spurious velocities are formed at the vicinity of the interface that in turn lead to unphysical fluctuations in the pressure field, causing unphysical movement of the interface during the bubble growth process. The adopted and implemented modification, involves the application of a smoothing procedure, prior to the calculation of the interface curvature. The predictions of the improved numerical model, are first validated against two different literature available experiments on adiabatic bubble growth and detachment from a submerged orifice. Then, the optimum version of the model is further applied for the conduction of a wide range of axisymmetric numerical simulations, aiming to quantitatively identify the exact influence of fundamental controlling parameters in the bubble detachment characteristics, for certain gravity levels that correspond to the majority of the planets on the solar system. The choice of the gravity levels of the planets is intended to give only a more pictorial representation of the results, but it does not result into a physical restriction of the final outcomes. Moreover, the effect of gravity vector inclination with respect to the air/vapor injection axis direction is examined, through a series of 3D numerical simulations. The supercomputing facilities of CINECA in Bologna, Italy, were utilized for the conduction of the large number of simulations, which were required for the present parametric investigations.

2. NUMERICAL METHOD

2.1 Governing equations

With the VOF approach, the transport equation for the volume fraction, α , of the secondary (dispersed) phase is solved simultaneously with a single set of continuity and Navier–Stokes equations for the whole flow field. The corresponding volume fraction of the primary phase is simply calculated as $(1 - \alpha)$. The main underlying assumptions are that the two fluids are Newtonian, incompressible, and immiscible. The governing equations can be written as:

$$\nabla \cdot \vec{U} = 0 \quad (1)$$

$$\frac{\partial \rho_b}{\partial t} + \nabla \cdot (\rho_b \vec{U}) = -\nabla p + \nabla \cdot \mu_b (\nabla \vec{U} + \nabla \vec{U}^T) + \rho_b f + F_s \quad (2)$$

$$\frac{\partial \alpha}{\partial t} + \nabla \cdot (\alpha \vec{U}) = 0 \quad (3)$$

where U is the fluid velocity, p the pressure, f the gravitational force, and F_s the volumetric representation of the surface tension force. The bulk density ρ_b and viscosity μ_b are computed as the averages over the two phases, weighted with the volume fraction α :

$$\rho_b = \rho \alpha + \hat{\rho}(1 - \alpha) \quad (4)$$

$$\mu_b = \mu \alpha + \hat{\mu}(1 - \alpha) \quad (5)$$

where ρ , $\hat{\rho}$, μ and $\hat{\mu}$, are the densities and the viscosities of the two phases. At this point it should be mentioned that the widely used, linear weighted average for the bulk viscosity calculation (equation 5), can be safely used for the physical problem that is addressed in the present investigation. In all of the simulated cases, two well defined bulks exist in the computational domain (gas/vapour and liquid) and the interface region. The interface region, the only region where any potential errors by the utilised bulk viscosity treatment could arise, is quite sharp (1 to 1.5 cells). Moreover, in all of the simulated cases of the present paper, a small bubble is tracked in a relatively large computational domain. Hence, even

for the largest density and viscosity ratios in the considered cases, the interface region in the overall computational domain represents a quite small percentage, and therefore this bulk viscosity treatment does not induce any considerable errors in the spatial and temporal evolution of the bubble growth and detachment. However, in other more complex physical problems such as bubbly flows with a large number of dispersed bubbles into the carrier liquid, other more complex treatments for the calculation of the bulk viscosity, should be utilised. In the VOF method, α is advected by the velocity field. For the case of incompressible flow, this is equivalent to volume fraction conservation, which makes the method mass conservative. Finally, the surface tension force is modelled as a volumetric force using the Continuum Surface Force (CSF) method by Brackbill et al. (1992) applying the following equations:

$$F_s = \gamma \kappa (\nabla \alpha) \quad (6)$$

$$\kappa = \nabla \cdot \left(\frac{\nabla \alpha}{|\nabla \alpha|} \right) \quad (7)$$

where γ is the tension of the interface and κ is the curvature of the interface.

2.2 Sharpening of the interface

Interface sharpening is very important in simulating two-phase flows of two immiscible fluids. In OpenFOAM the sharpening of the interface is achieved artificially by introducing an extra compression term in the advection equation of α . Therefore equation (3) is modified and transformed to the following equation:

$$\frac{\partial \alpha}{\partial t} + \nabla \cdot (\alpha \vec{U}) - \nabla \cdot (\alpha(1 - \alpha) \vec{U}_r) = 0 \quad (8)$$

\vec{U}_r is the artificial compression velocity which is calculated from the following relationship:

$$\vec{U}_r = n_f \min \left[C_\gamma \frac{|\varphi|}{S_f}, \max \left(\frac{|\varphi|}{S_f} \right) \right] \quad (9)$$

where n_f is the cell surface normal vector, φ is the mass flux, S_f is the surface area of the cell, and C_γ is a coefficient, the value of which can be set between 0 and 4. \vec{U}_r is the relative velocity between the two fluids due to the density and viscosity change across the interface. In equation (8) the divergence of the compression velocity \vec{U}_r , ensures the conservation of the volume fraction α , while the term $\alpha(1-\alpha)$ limits this artificial compression approach only in the vicinity of the interface, where $0 < \alpha < 1$ (Hoang et al., 2013). The level of compression depends on the value of C_γ (Deshpande et al., 2012; Hoang et al., 2013). For the simulations of the present paper, initial, trial simulations indicated that a value of $C_\gamma=1$ should be used, in order to maintain a quite sharp interface without at the same time having unphysical results.

2.3 VOF Smoothing

As it is known the VOF method usually suffers from non-physical spurious currents in the interface region. These spurious velocities are due to errors in the calculation of the normal vectors and the curvature of the interface that are used for the calculation of the interfacial forces. These errors emerge from the fact that in the VOF method the interface is implicitly represented by the volume fraction values that encounter sharp changes over a thin region (Scardovelli and Zaleski, 1999). In the present paper initially, following the treatment of Hoang et al. (2013) the spurious currents are suppressed by suitably modifying the original VOF-based solver of OpenFOAM (interFoam). The proposed modification involves the calculation

of the interface curvature κ using the smoothed volume fraction values $\tilde{\alpha}$, which are obtained from the initially calculated α field, smoothing it over a finite region in the vicinity of the interface. All other equations are using the initially calculated (non-smoothed) volume fraction values of α . Therefore, instead of equation (7) the following equation is used for the interface curvature calculation:

$$\kappa = \nabla \cdot \left(\frac{\nabla \alpha}{|\nabla \alpha|} \right) \quad (10)$$

The proposed smoothing is achieved by the application of a Laplacian filter which can be described by the following equation:

$$\tilde{\alpha}_P = \frac{\sum \alpha_f s_f}{\sum s_f} \quad (11)$$

In Equation (11), the subscripts P and f denote the cell and face index respectively and α_f is the linearly interpolated value of α at the face center. The application of the proposed filter can be repeated more than one time in order to obtain an adequately smoothed field. For the applications of the present investigation, initial trial simulations indicated that this filter should be applied no more than 2 times, in order to avoid the leveling out of high curvature regions.

In order to test the degree of spurious current dampening for the modified solver, the widely used Brackbill's test case is used (Brackbill et al., 1992). In this test case a cuboidal bubble is initially patched at a stagnant liquid domain of different density and viscosity, with no gravity effects taken into consideration, and it is let to reach its equilibrium state. At this equilibrium state a spherical bubble should be formed at rest in the center of the computational domain with a pressure difference with the ambient liquid, equal to the Laplace pressure difference. Figure 1 (a) depicts the results of the maximum velocity in the computational domain with respect to time, for the modified and the original VOF solver of OpenFOAM, while Figure 1 (b) shows the numerically predicted pressure difference between the relaxed spherical bubble and the ambient liquid along the bubble diameter axis for each of the two cases, in comparison with the theoretical value predicted from the Laplace equation. As it can be observed the modified/improved VOF solver that is adopted for the applications of the present investigation ("VOF-Smooth" in the figure legend) reduces significantly the spurious velocities (Figure 1a) and it also provides a better prediction of the theoretical pressure difference (Figure 1b) than the original VOF solver of OpenFOAM ("VOF" in the figure legend). Finally, in Figure 1c, the effect of the proposed smoothing treatment in a real bubble case is depicted. In more detail the volume fraction, the relative pressure and velocity field (superimposed in the corresponding pressure field), are plotted in a central vertical section of the computational domain, for the case of a bubble that is formed by the quasi-static air injection from a submerged orifice, into an isothermal water pool. As it can be observed, in the case where no smoothing has been applied, despite the fact that the interface is sharp and well-defined, spurious fluctuations are observed in the relative pressure field due to the corresponding spurious velocities development in the vicinity of the interface (VOF case). On the contrary, in the case that the smoothing procedure has been applied, these spurious fluctuations in the relative pressure and velocity fields are not present any more, while the interface still remains sharp and well-defined (VOF-Smooth case).

2.4 Simulation Parameters

As mentioned previously, all the numerical simulations on adiabatic bubble growth and detachment of the present work were performed with the finite-volume-based CFD code OpenFOAM (version 2.2.1) utilizing and improving the VOF-based solver "interFoam". For pressure-velocity coupling, the PISO (pressure-implicit with splitting of operators) scheme is

applied. The transient terms in the equations are discretized using a second order, bounded, implicit scheme (CrankNicolson). The calculation time step is controlled by setting the maximum Courant number to 0.2. With this adaptive time stepping technique, the time step was automatically varied from approximately 10^{-6} to 10^{-5} sec. The gradient terms are discretized using a second order, Gaussian integration with linear interpolation (Gauss linear). For the divergence terms different discretization schemes are applied for each term in the equations. In more detail the convection term of equation (2) is discretized using a Gauss limited linear scheme in order to produce good accuracy, with the value of the required coefficient ϕ equal to unity, since this value ensured better stability during the calculations (Gauss limitedLinearV 1.0). The $\nabla \cdot (\alpha \bar{U})$ term of equation (8) is discretised using the “Gauss vanLeer” scheme, while the $\nabla \cdot (\alpha(1 - \alpha)U_x)$ term is discretised using the “Gauss interfaceCompression” scheme that ensures the boundedness of the calculated volume fraction field. Finally, all Laplacian terms are discretised using the “Gauss Linear Corrected” scheme. Further details regarding the adopted discretization schemes can be found in OpenFOAM Documentation (OpenFOAM, 2013).

For the axisymmetric simulations of the present paper, a uniform hybrid computational mesh, consisting of hexahedral and prismatic elements was used, while for the 3D simulations the computational mesh was non-uniform consisting of hexahedral, prismatic and polyhedral elements, with different levels of refinement. The finer mesh region was extended symmetrically in all directions from the inlet boundary, up to a certain distance so that the whole bubble growth and detachment process to occur within it. Mesh independence studies indicated that the solution is mesh-independent if 32 computational cells are used within the inlet diameter, in each case. This also agrees with previous similar investigations (e.g. Albadawi et al., 2012; Albadawi et al., 2013a, 2013b). At the solid walls, a no-slip velocity boundary condition was used with a fixed flux pressure boundary condition for the pressure values and a constant contact angle boundary condition for the volume fraction values. This contact angle boundary condition is used to correct the surface normal vector, and therefore adjusts the curvature of the interface in the vicinity of the wall in relation to the wettability of the solid material. A parabolic inflow velocity profile, a fixed flux pressure and a constant volume fraction value were applied at the inlets. At the outlet, a fixed-valued (atmospheric) pressure boundary condition and a zero-gradient boundary condition for the volume fraction were used, while for the velocity values a special (combined) type of boundary condition was used that applies a zero-gradient when the fluid mixture exits the computational domain and a fixed value condition to the tangential velocity component, in cases that fluid enters the domain. Further details regarding the utilized boundary conditions can be found in OpenFOAM Documentation (OpenFOAM, 2013).

3. VALIDATION OF NUMERICAL METHOD

3.1 Problem Definition

In order to validate the numerical model, initially the experiments on quasi-static bubble growth and detachment reported in the recent work of Albadawi et al. (2013b) were selected among others as “Validation Case 1”, since many necessary information for their numerical reproduction are reported by the authors. In more detail, the formation of air bubbles at an orifice in a stagnant water domain is considered. The gas phase is injected through the orifice using a small and constant volumetric flow rate Q , so that the bubble growth and detachment process can be considered to fall in the quasi-static regime.

The proposed experimental facility consists of a horizontal surface from which bubble growth takes place through a stainless steel orifice of 1.6 mm diameter, submerged to a depth of 20 mm below the surface of water within a square 50 mm glass tank. Gas flow rate is controlled with the combination of a Hamilton (GASTIGHT 1002 series) 2.5 ml syringe and a kdScientific (KDS 200 cz) infusion pump. A single NAC Hi-Dcam II high speed digital video camera is used to capture images at a frame rate of 1000 Hz, with an exposure time of 0.5 ms which results in quite sharp images. The bubble was

illuminated with a diffused back light, consisting of six 300 lm LED bulbs in an array. In order to detect the boundary of the bubble, a custom image processing code has been developed, which utilizes the Image processing toolbox developed by Matlab. Raw images were converted from the RGB to the HSV color space. The boundary of the bubble was then detected by means of bubble isolation. According to the authors (Albadawi et al., 2013b), this isolation method results in an uncertainty in detecting the bubble boundary of \pm one pixel, which corresponds to a value of ± 0.0134 mm.

3.2 Computational setup

Since, the process of bubble growth and detachment in these experiments can be considered to be axisymmetric, an axisymmetric computational domain was constructed for their numerical reproduction. As also mentioned in the previous section of the present paper, mesh dependency studies indicated that the numerical solution can be considered to be mesh-independent with 16 computational cells per orifice radius. The adopted computational domain, mesh and boundary conditions are illustrated in Figure 2. As it can be seen, a wedge type geometry was constructed representing a 5 degrees section of the corresponding 3D domain of the considered physical problem. A uniform computational mesh was used consisting of 79,600 hexahedral cells and 400 prismatic cells in the vicinity of the axis of symmetry. A cell size of 50 μ m was selected in order for the solution to be mesh-independent. The overall domain size in the XY plane is 10 mm x 20 mm. These dimensions were indicated from initial, trial simulations that were conducted in order to determine the minimum distances between the inlet and the perpendicular wall boundary as well as between the inlet and the outlet, in order to avoid any influence of these boundaries in the computed bubble growth and detachment process.

At the inlet, the flow is assumed to be fully developed, laminar and a parabolic inflow velocity profile is imposed applying the following relationship at the inlet boundary:

$$u = u_{max} \left(1 - \frac{x^2}{R_c^2} \right) \quad (12)$$

where at $x=0$ (axis of symmetry) the velocity takes its maximum value v_{max} and at $x=R_c$ (orifice diameter) the velocity becomes zero. The maximum velocity value is calculated from the volumetric injection flow rate Q as:

$$u_{max} = \frac{2Q}{\pi R_c^2} \quad (13)$$

At the lower wall an equilibrium contact angle is imposed as $\theta=20^\circ$. The contact angle θ is used in order to calculate the surface normal (\vec{n}) in the adjacent to the wall boundaries computational cells, where the two fluid phases are in direct contact with the solid surface, utilizing the following relationship:

$$\vec{n} = \vec{n}_n \cos \theta + \vec{n}_t \cos \vartheta \quad (14)$$

where \vec{n}_n and \vec{n}_t are the unit vectors at the directions normal and tangential to the solid wall, respectively (Ubbink, 1997).

The equilibrium contact angle for air, water and stainless steel can vary depending on the water purity as well as the surface cleanliness, roughness and wettability. However, it has been shown by Gerlach et al. (2007) that if in a numerical simulation, the imposed contact angle is below a limiting value, the evolving interface between the forming bubble and the ambient liquid stays pinned at the orifice rim. At this point it should be mentioned that initial trial simulations verified that imposing angles lower than 20° does not influence significantly the bubble detachment characteristics, and the interface

between the two phases remains attached to the orifice during the entire process of the bubble growth. Here the value of 20° was selected in order for the interface to stay pinned at the orifice as observed in the proposed experiments (Albadawi et al., 2013b). The initial conditions that are used for the considered numerical validation case, imitating the corresponding experimental conditions are summarized in Table 1 (Case 1).

3.3 Comparison of numerical and experimental results

In Figure 3, a quantitative comparison is made by extracting the point coordinates of the interface position with respect to time, both from the numerical and the corresponding experimental results, from the beginning of the considered phenomenon up to a time just before the bubble detachment from the orifice. At each time instance, a macroscopic qualitative comparison is also included, illustrating side by side (at the same time instances) the reconstructed 3D evolution of the 0.5 volume fraction contour (interface) from the axisymmetric simulation and the corresponding experimental snapshots. As it can be observed, there is an excellent convergence of the numerical and the experimental results. The spatial evolution of the numerically predicted interface is very close to the corresponding experimental data, in each of the considered time intervals, before the detachment of the bubble from the orifice. However, a small difference in the predicted and measured time values that are considered here as the time of detachment can be observed. This deviation at the predicted time of detachment may arise both from the overall numerical assumptions as well as from the experimental uncertainties. However, as it can be seen from Table 2, the modified VOF solver for spurious current reduction that was used in the present paper, predicts the bubble detachment characteristics much closer to the experimental values than other non-modified VOF solvers that were tested and reported in the work of Albadawi et al. (2013).

Since, in the work of Albadawi et al. (2013b) no experimental data are reported regarding the interface evolution after the bubble detachment, it was deemed appropriate to check the numerical predictions of the present numerical model, through a second validation case (Validation Case 2), reproducing numerically the experiments that are presented in the work of Quan and Hua (2008). The same simulation characteristics as well as the same computational domain and mesh were used, as in the previously presented validation case (Validation Case 1). The only difference was the orifice radius as well as the initial conditions that are also summarized in Table 1 (Case 2).

In Figures 4 and 5, a quantitative comparison is made by extracting the point coordinates of the interface position with respect to time, both from the numerical (present investigation) and experimental results (Quan and Hua, 2008), at certain time instances before (Figure 4) and after (Figure 5) the detachment of the bubble from the orifice. As previously (Validation Case 1), for all the depicted times, a macroscopic qualitative comparison is also included, through the comparison of the reconstructed 3D evolution of the 0.5 volume fraction contour (interface) from the axisymmetric simulation, with the corresponding experimental snapshots (bottom left part in these figures). As it can be observed, the results of the present numerical model are in excellent agreement with the proposed experimental results, considering the successive shape transitions of the generated bubble, both before and after the time of detachment from the orifice. Therefore, it can be concluded that the improved VOF-based numerical model that is proposed and used in the present paper, can be safely utilized for the conduction of numerical experiments that aim in the investigation and understanding of the underlying dynamics in cases of adiabatic gas/vapor bubbles that grow quasi-statically and detach from submerged orifices, in liquid pools. However, it should be stated here that the proposed and utilized treatment for spurious currents dampening, cannot be considered as a global treatment for the simulation of a wider range of physical problems, were the interface between two incompressible and immiscible fluids needs to be tracked. Therefore, it is

suggested that for different physical problems, this smoothing treatment as well as the number of times that the proposed filter must be applied, should always be checked against analogous experimental data.

4. EFFECT OF FLUID PROPERTIES

In the present section of the paper, the improved and validated VOF model that was described and validated against literature available experiments in the preceding section, is further applied in order to investigate the effect of fluid properties in the bubble detachment characteristics. Initially, in order to visualise the influence of the fluid properties on the bubble growth and detachment characteristics, one of the numerical simulation cases described in the previous section of the paper (Validation case 1) is further applied, keeping the same initial conditions but changing the fluid properties of the two-phase system. In more detail, two additional numerical simulations are performed using the saturation values of vapour and liquid properties for R245fa and Decane, at atmospheric pressure, instead of water and air that was used in the experiments of Albadawi et al. (2013b). The utilized properties for these additional simulations are summarized in Table 3.

In Figure 6, a comparison of the bubble growth and detachment process is made between these two additional simulations and the initial Water/Air case that was used for the validation of the numerical model (Validation case 1). In each case, streamlines in a central vertical section of the flow field (coloured by the velocity magnitude) are illustrated, in conjunction with the 3D evolution of the interface, between the gas/vapor and liquid phases (transparent grey surface, reconstructed as the 0.5 volume fraction iso-surface), for three successive time instances. One at an earlier time prior the detachment of the bubble, one just before the detachment (final stage of bubble necking), and one a few msec after the pinch-off of the bubble. The equivalent bubble detachment diameter (D_{eq}) and the bubble detachment time (t_{det}), are also indicated for each case. The equivalent bubble detachment diameter is calculated as the diameter of a sphere that has the same volume, as the volume of the bubble at detachment. The time of detachment is considered as the time instance just prior to the bubble pinch-off from the orifice. As it can be observed, the bubble growth and detachment characteristics are strongly dependent on the fluid properties. Despite the fact that in all cases the gas/vapour injection rate, the orifice diameter and the static contact angle values are kept constant, it is evident that in the R245fa case the detachment time and volume are significantly smaller than in the Water/Air case, while the Decane case presents quite higher bubble detachment characteristics. Comparing the equivalent bubble detachment diameters between the two additional simulations, it is characteristic that in the Decane case, the bubble detaches from the orifice with almost the double diameter as that of the R245fa case. Furthermore, it is evident that the shape evolution of the interface is quite different in all three cases. For example, the rising bubble after the pinch-off from the orifice, in the case of Decane, maintains a more spherical shape than the concave shape at the bottom of the bubble that is observed in the other two cases. It is also quite interesting that in the case of R245fa, at the early stage of the bubble growth, the growing bubble encounters a more elongated bullet-like shape, which is not observed in the other two cases. Another quite interesting observation that results by the examination of the streamline field, is the formation of Worthington jets that are formed after the bubble detachment from the orifice, in agreement with previous investigations (Chakraborty et al., 2011). Finally, in all cases the formation of recirculation regions in the flow domain is evident. However, despite the fact that the same injection flow rate and orifice diameter is used, the size, shape and core position of these regions is quite different in each of the examined cases. All these macroscopic observations, clearly identify the importance of variable fluid properties, such as surface tension, density and viscosity in the bubble growth and detachment characteristics.

In all three cases of Figure 6, the gas injection is under a constant flow rate of $Q = 4.17 \times 10^{-8} \text{ m}^3/\text{s}$ which is lower than the critical value for quasi-static bubble growth ($Q_{crit} = \pi \left(\frac{16}{3g^2} \right)^{1/6} \left(\frac{\sigma R_0}{\rho_l} \right)$) identified by Oguz and Prosperetti (1993). The corresponding critical values for the R245fa, Water/Air and Decane cases are 3.82×10^{-7} , 1.82×10^{-6} and $9.68 \times 10^{-7} \text{ m}^3/\text{s}$, respectively. As it is mentioned before, in the introduction section of the present paper, since the gas flow rate is in each case well below the corresponding critical values, the numerically predicted bubble detachment diameter should remain almost constant by further increasing or decreasing the gas/vapour injection flow rate. In order to check this, the R245fa case is further modified by performing two additional simulations where the imposed vapour injection flow rate is successively increased from 150 (Figure 6) to 200 and 300 mlph. In Figure 7, the R245fa case that was previously compared with the Water/Air and the Decane cases, is now compared with these two additional cases of successively higher vapour injection flow rates.

As it can be observed, despite the increase of the considered in each case vapour injection flow rate, the equivalent bubble detachment diameter stays almost constant. It is characteristic that increasing the flow rate by a factor of 2 (comparing the two extreme cases), the equivalent bubble detachment diameter increases insignificantly by a factor of just 1.04. However, the bubble detachment time decreases by a considerable factor of 1.63. Therefore, in agreement with previous investigations, it can be concluded that for quasi-static bubble growth from submerged orifices into isothermal liquid pools, the influence of the gas injection flow rate to the bubble detachment diameter is negligible, while the influence of fluid properties is quite important. Therefore, the remaining part of the present section of the paper, will focus on the effect of variable fluid properties as well as of variable gravity levels on the equivalent bubble detachment diameter and the bubble detachment time.

In order to further investigate the exact quantitative effect of fundamental controlling parameters on the bubble detachment characteristics, such as the fluid properties as well as the gravitational acceleration, five additional series of parametric numerical simulations with variable fluid properties are performed, for five different gravity levels that correspond to the gravitational acceleration values of all the major planets in the Earth's solar system. In more detail, parametric runs are conducted in each series varying the fluid properties of the R245fa case presented earlier (see Figure 6a). In each series, in the first six simulations the value of the surface tension coefficient is varied (range: 0.01 to 0.06 N/m), while all the other properties are kept constant with respect to the base case. In the following six simulations the density (range: 250 to 1600 kg/m^3) and accordingly the kinematic viscosity values of the liquid phase are varied, keeping the dynamic viscosity and the rest of the properties unchanged. Finally, in the last 10 simulations of each series the values of the liquid phase dynamic and accordingly kinematic viscosity are varied (low viscosity range: 1×10^{-4} to $2 \times 10^{-3} \text{ kg}/\text{m s}$, high viscosity range: 0.025 to 0.1 $\text{kg}/\text{m s}$), keeping the liquid density and the rest of the properties constant. The initial conditions of the base case as well as the overall varied parameters for the 115 in total additional simulations, are summarized in Table 4. At this point it should be mentioned that the R245fa case was selected as the base case for the proposed parametric investigation, since as it can be observed from Figure 6a, it has the lowest bubble detachment characteristics (diameter and time) and hence the lowest computational demand, especially from the computational time point of view.

A schematic representation of the effect of each of the examined fundamental controlling parameters (gravitational acceleration, surface tension, liquid phase density and liquid phase dynamic viscosity) on the bubble detachment volume, is depicted in Figures 8a to 8d, respectively. In all these figures, the position of the interface between the generated in each case vapour bubble and the ambient liquid, is illustrated in a central XY plane of the reconstructed 3D

flow field from the axisymmetric simulations, for the time instance just before the bubble detachment from the orifice. The predicted in each case equivalent bubble detachment diameter and bubble detachment time, are also shown in the corresponding figure legends. It should be mentioned that in all of the simulated cases, the latter in each simulation time instance, just before the bubble pinch-off from the orifice, is considered as the bubble detachment time, at which the equivalent bubble detachment diameter is calculated by equating the generated bubble volume to the volume of a sphere. Furthermore, the bubble detachment characteristics, for all cases presented in Figure 8, are plotted in Figures 9a to 9d, against the varied parameter in each case, being normalized by their corresponding reference values. The result of the reference numerical simulation in each case is represented by the blue line in Figures 8a to 8b and is also highlighted with a red circle in the diagrams of Figure 9. The fluid properties variation ranges that are shown in Table 4, are applied in all of the considered gravity levels that are illustrated in Figures 8a and 9a. However, at this stage the effect of surface tension variation is depicted indicatively only for the gravity level of Earth (Figures 8b and 9b) and accordingly the effects of the liquid phase density (Figured 8c and 9c) and liquid phase dynamic viscosity (Figures 8d and 9d), only for the gravity levels of Venus/Saturn/Uranus and Neptune, respectively. As it can be observed from Figure 8a, the variation of the gravitational acceleration has a direct influence on the bubble detachment volume. In general, as the value of the gravitational acceleration decreases the bubble detachment volume increases. This can be explained by considering the magnitude of the buoyancy force in the bubble. A decrease in the gravitational acceleration induces a subsequent decrease in the buoyancy force. Therefore in order for the buoyancy force magnitude to become significant and aid to the detachment of the bubble from the orifice, a higher bubble volume must be attained. For planets of a similar gravity level with Earth (Neptune, Venus, Saturn and Uranus) the influence is minimal, while for planets with significantly lower gravity level (Mars, Mercury and Pluto) the effect in bubble detachment volume is quite significant. In more detail, it is evident that increasing the reference gravitational acceleration (Earth) by a factor of 1.12 (Neptune) or decreasing it by a factor of 1.11 (Venus/Saturn/Uranus), the equivalent bubble detachment diameter decreases and increases, respectively, by a factor of just 1.03. However, the bubble detachment time decreases and increases accordingly by a considerable factor, of approximately 1.13. Further decreasing the reference gravitational acceleration (Earth) by a factor of 2.64 (Mars/Mercury) and 16.91(Pluto), the equivalent bubble detachment diameter increases by a factor 1.33 and 2.71 respectively, while the bubble detachment time increases by much higher factors of 2.71 and 14.97. From Figure 9a, it is evident that both the equivalent bubble detachment diameter as well as the bubble detachment time follow a power law increase with the corresponding decrease of the gravitational acceleration. However, the influence of the gravitational acceleration variation, is quite more significant in the bubble detachment time.

Regarding the effect of surface tension, Figure 8b indicates that for the Earth's gravity acceleration that is considered, in general a successive increase of the surface tension value causes a similar increase in the bubble detachment volume. This happens, since an increase in the surface tension value, causes a subsequent increase in the surface tension force that is the main force that tends to keep the bubble attached to the orifice. Therefore, in order for the bubble to detach a higher bubble volume is required in order for the buoyancy force to become significant and lead to the detachment of the bubble. It can be seen that in comparison with the reference case ($\sigma = 0.015 \text{ N/m}$), a decrease in the surface tension value by a factor of 1.50, causes a corresponding decrease in the equivalent bubble detachment diameter and the bubble detachment time by a factor of 1.10 and 1.51, respectively. Moreover, a successive increase of the surface tension value by a factor of 1.33, 2.00, 2.67, 3.33 and 4.00, increases the equivalent bubble detachment diameter by a corresponding factor of 1.07, 1.20, 1.31, 1.39 and 1.46, and the bubble detachment time by 1.31, 1.94, 2.54, 3.09 and 3.67, respectively. From Figure 9b, it can be seen that both the equivalent bubble detachment diameter as well as the bubble

detachment time, follow a linear increase with the corresponding increase in the value of the surface tension. However, again the influence is much higher in the bubble detachment time.

Figure 8c indicates that for the considered gravity level (Venus/Saturn/Uranus), the liquid phase density is also an important influencing parameter on the bubble detachment characteristics. Generally, a decrease in the value of the liquid phase density causes a corresponding increase in the bubble detachment characteristics. This happens, since a decrease in the liquid phase density causes a corresponding decrease in the density difference between the two phases, and therefore the bubble must reach to a larger volume, in order for the magnitude of the buoyancy force to become important and lead to its detachment from the orifice. In more detail, increasing the reference value ($\rho_l = 1364.9 \text{ kg/m}^3$) by a factor of 1.1 and 1.17, the equivalent bubble detachment diameter decreases by a factor of 1.02 and 1.04, respectively, while the bubble detachment time also decreases by a factor of 1.1 and 1.17. Furthermore, a successive decrease of the liquid phase density by a factor of 1.36, 1.82, 2.73 and 5.46, increases the equivalent bubble detachment diameter by a corresponding factor of 1.09, 1.18, 1.32 and 1.62, and the bubble detachment time by a corresponding factor of 1.35, 1.79, 2.60, and 5.06, respectively. From Figure 9c, it is evident that both the equivalent bubble detachment diameter as well as the bubble detachment time, follow a power law decay with the increase of the liquid phase density, as it is indicated by the data plots and their corresponding power fits. Here again, it is evident that the variation of the considered controlling parameter, has a bigger effect in the bubble detachment time and a smaller but still considerable effect in the equivalent bubble detachment diameter.

Finally, the influence of the liquid phase dynamic viscosity on the bubble detachment characteristics is addressed in Figures 8d and 9d. In this case, an interesting observation is that for small variations of the reference value ($\mu_l = 0.00046 \text{ kg/m s}$), both the equivalent bubble detachment diameter and the bubble detachment time remain almost constant. In more detail, decreasing the reference value by a factor of 2.00 and 4.00 respectively, or increasing it by a factor of 1.74, 1.96, 2.17 and 4.35 the equivalent bubble detachment diameter and the bubble detachment time change by a maximum factor of just 1.01 and 1.06, respectively. Furthermore, even for a quite high increase of the reference dynamic viscosity value by a factor of 217, the equivalent bubble detachment diameter and the bubble detachment time increase only by a factor of 1.21 and 2.00, respectively.

From the analysis and discussion of the results so far, it can be concluded that the gravitational acceleration, the surface tension as well as the liquid phase density, influence significantly the bubble detachment characteristics and especially the bubble detachment time. On the contrary, in comparison to the influence of the aforementioned controlling parameters, the variation of the liquid phase dynamic viscosity has a minimal effect both in the equivalent bubble detachment diameter as well as in the bubble detachment time. Comparing the diagrams of Figure 9, it is evident that the most influential parameter, especially in the bubble detachment time, is the gravitational acceleration, while the effects of the surface tension and the liquid phase density are of quite similar magnitude. However, despite the fact that similar gravity levels are used in Figures 8b to 8d as well as in Figures 9b to 9d, in order to compare the corresponding influences of the examined fluid properties to the bubble detachment characteristics in a more detailed and comprehensive way, the diagrams illustrated in Figure 10 are plotted. In more detail, in Figures 10a, 10b and 10c, the dimensionless equivalent bubble detachment diameter (dimensionalized by the diameter of the vapour injection orifice D_0) is plotted against the surface tension, liquid phase density and dynamic viscosity values, respectively, for all of the considered gravity levels. For comparison purposes, the values of the varied parameters are normalized by their reference value in each of the considered gravity levels. Accordingly, in Figures 10d, 10e and 10f, the dimensionless bubble detachment time (dimensionalized by multiplying each value by the ratio of the gas injection velocity to the

orifice diameter U_0/D_0), is plotted against the aforementioned normalized values of the examined properties, for all the considered gravity levels. As it can be observed from Figure 10a, the linear increase of the equivalent bubble detachment diameter with the increase of the surface tension that was shown in Figure 9b for the gravity level of Earth, is also evident in the rest of the considered gravity levels. However, as the gravity level successively reduces to significantly lower values (3.71 and 0.58 m/s^2), apart from the expected higher values in the equivalent bubble detachment diameter, a successive increase in the slope of the aforementioned linear trend is also evident. These observations are even more significant for the bubble detachment time (Figure 10d).

Similarly, carefully observing Figures 10b and 10e, the power law decay of the bubble detachment characteristics with the increase of the liquid phase density that was illustrated in Figure 9c for the gravity levels of Venus, Saturn and Uranus, is also evident in the rest of the considered gravity levels. Again here, as the gravity level significantly reduces with respect to the gravitational acceleration of the Earth, the bubble detachment characteristics show significantly higher values and their rate of increase with respect to the corresponding decrease of the liquid phase density becomes successively higher. Also here, these observations are more significant to the bubble detachment time in comparison to the equivalent bubble detachment diameter.

Finally, regarding the influence of the liquid dynamic viscosity on the bubble detachment characteristics that is depicted in Figures 10c and 10f, the negligible linear increase of the equivalent bubble detachment diameter and the bubble detachment time with respect to the considerable increase of the liquid phase dynamic viscosity, that was observed in Figure 9d for the gravity level of Neptune, is also present for the rest of the considered gravity levels. However, for the lowest of the examined gravity levels (Pluto), it is characteristic that for the low variation range of the reference dynamic viscosity value (Table 4), that in the rest of the considered gravitational accelerations its effect on the bubble detachment characteristics is negligible, in this case both the equivalent bubble detachment diameter as well as the bubble detachment time present a quite rapid and considerable in magnitude increase.

Table 5, summarises the maximum change factor in the equivalent bubble detachment diameter as well as in the bubble detachment time, in comparison with the maximum variation factor of all of the three examined fluid properties in the present parametric investigation, for each of the considered gravity levels. The maximum variation factors are calculated as the ratio of the highest to the lowest values from the overall variation range of the examined fluid properties.

As it was observed from the diagrams of Figure 10, it is evident also from Table 5 that the liquid phase viscosity effect on the bubble detachment characteristics is minimal in comparison to the rest of the examined fluid properties. Comparing now the resulting maximum change factors with respect to the maximum variation factors for the surface tension and the liquid phase density, it is obvious that their corresponding effect in the equivalent bubble detachment diameter is almost the same. However, the influence of the liquid phase density is a bit higher than the corresponding influence of the surface tension, in the bubble detachment time. Another quite interesting observation is the fact that the maximum change factors in the bubble detachment characteristics with respect to the maximum variation factors of the considered flow properties, present similar values for gravity levels (10.99 m/s^2 and 8.83 m/s^2) close to the reference gravity level (9.81 m/s^2). However, as the gravity level significantly deviates from the reference value (3.71 m/s^2 and 0.58 m/s^2), the maximum change factors increase or decrease accordingly, significantly with respect to the maximum change factor in the case of the reference gravitational acceleration.

In the quasi-static bubble growth regime, as a first-order assessment, a simple force balance between buoyancy and surface tension forces just before the detachment from the orifice, can be applied. In other words, in this case the bubble is considered to detach from the orifice when the buoyancy force exceeds the maximum possible surface tension force. This can be expressed by the following equation:

$$F_B = F_S \Rightarrow \frac{\pi}{6} D_{eq}^3 (\rho_l - \rho_g) g = \pi D_0 \sigma \quad (15)$$

Rearranging equation (15), the following theoretical correlation that predicts the equivalent bubble detachment diameter in relation to the Eötvös number (or equivalently the Bond number “Bo”) is derived:

$$\frac{D_{eq}}{D_0} = 1.82 E_o^{-0.33} \quad (16)$$

where the Eötvös number is defined as follows:

$$E_o = \frac{(\rho_l - \rho_g) g D_0^2}{\sigma} \quad (17)$$

The proposed theoretical correlation, has served so far in the literature as the “conventional prototype” for the prediction of the equivalent bubble detachment diameter, for isolated bubbles, growing and detaching from submerged orifices in isothermal liquid pools, while being in the quasi-static growth regime (Di Marco, 2005; Dietrich et al., 2013; Kulkarni and Joshi, 2005).

As it can be observed from Figure 11, by plotting the numerically predicted equivalent bubble detachment diameters (blue coloured data) for all the numerical simulations of the present parametric investigation, normalized by the orifice diameter (D_0), against the calculated Eötvös numbers in a logarithmic scale, but excluding the high range values of the liquid phase dynamic viscosity variation (please see Table 4), the following power law relationship is found to best describe the numerically derived data:

$$\frac{D_{eq}}{D_0} = 1.68 E_o^{-0.29} \quad (18)$$

By utilizing Equation (16) and plotting also the theoretical equivalent bubble detachment diameters in the same graph (brown coloured data), a quite significant deviation from the numerically predicted data can be observed. In more detail, the proposed deviation increases in magnitude as the Eötvös number reduces. The low range of Eötvös numbers, where the more significant deviations are observed, correspond to the lowest of the examined gravity levels ($g= 0.58 \text{ m/s}^2$), in the conducted parametric numerical simulations. As it was illustrated previously in Figure 10c, for the low value range of the liquid dynamic viscosity (μ_l : 0.001-0.002 kg/m s) and for the lowest of the examined gravity levels ($g= 0.58 \text{ m/s}^2$), the effect of liquid phase viscosity in the equivalent bubble detachment diameter is quite significant in comparison to the rest of the examined gravity levels that the corresponding influence is negligible. Therefore, since the aforementioned theoretical correlation safely neglects the influence of viscosity for gravity levels close to the value of Earth, it fails to capture the aforementioned irregularity for very low gravity levels and hence deviates significantly from the numerically predicted data. This suggests that the proposed theoretical correlation (Equation 16) that is derived

by the a simplified force balance (Equation 15) should be further modified, applying a suitable correction that takes into account a combination of the viscosity and gravity effects on the bubble detachment characteristics. Here the following correction is suggested:

$$\frac{D_{eq}}{D_0} = 1.82E0^{-0.22} \left(\frac{g}{g_{Earth}} \right)^{0.06} \left(\frac{\mu}{\mu_{water}} \right)^{0.02} \quad (19)$$

By plotting also Equation (19) in the diagram of Figure 11, the green coloured data points are derived. As it can be observed their best fit line that is described by Equation (20) below, is very close to the corresponding equation of the best fit line of the numerically predicted data (Equation 18):

$$\frac{D_{eq}}{D_0} = 1.74E0^{-0.22} \quad (20)$$

Therefore, it can be concluded that for the quasi-static bubble growth regime and for the considered ranges of gravity levels, surface tension coefficients, liquid phase densities and liquid phase dynamic viscosities, Equation (19) can be safely applied for the prediction of the equivalent bubble detachment diameter, taking into account all the fundamental controlling parameters that were identified as influential, in the present parametric analysis.

In Figure 12, the numerically predicted equivalent bubble detachment diameters, normalized by the orifice diameter, are plotted against the calculated Eötvös numbers for all of the conducted numerical simulations of the present parametric analysis, including also the high dynamic viscosity range runs (please see Table 4). However, in order to highlight the deviation from the power law fit of Equation (18) that resulted previously (Figure 10, blue coloured data), the high viscosity runs are grouped together by the liquid dynamic viscosity value and are plotted with separate colours. As it can be observed, the previously identified fit of Equation (18), is successively shifted as higher levels of viscosity are considered. This clearly shows that towards the prediction of the bubble detachment diameter for quasi-static bubble growth, two different regimes can be identified. A regime of “low-viscosity” fluids where the bubble detachment diameter can be globally predicted by a single power law for a wide range of Eötvös numbers, and a “high-viscosity” fluids regime where successive increase in liquid viscosity values cannot be described by a single power law relationship.

Finally, in accordance to Figure 12, in Figure 13, the variation of the numerically predicted bubble detachment time (normalized by multiplying the corresponding values by the ratio of the gas injection velocity to the orifice diameter U_0/D_0), with respect to the Eötvös number is plotted. As it can be observed, considering all the conducted numerical simulations but excluding the high viscosity runs, the bubble detachment time can be predicted by the following relationship that results from the equation of the corresponding best fit curve:

$$\frac{t_{det}U_0}{D_0} = 2.88E0^{-0.95} \quad (21)$$

As in the case of the equivalent bubble detachment diameter, it is obvious that the resulting fit of equation (21) is successively shifted as higher levels of viscosity are considered. This again indicates that towards the prediction of the bubble detachment time, the same two different viscosity regimes can be identified.

5. EFFECT OF GRAVITY VECTOR INCLINATION ANGLE

In this section of the paper, the effect of the gravity vector inclination angle with respect to the horizontal plane in the bubble growth and detachment characteristics is investigated. For this purpose a full, 3D, cylindrical computational domain is constructed. The computational domain, mesh and the applied boundary conditions are illustrated in Figure 14. As it can be seen, a non-uniform computational mesh is used with three levels of mesh refinement. The finer mesh region covers the volume that the bubble growth and detachment takes place, identified by the axisymmetric simulation of R245fa that was presented and discussed in the previous section of the present paper (Section 4, Figure 6a). The reason that the 3D numerical investigation is conducted for the R245fa case is simply for computational speed purposes, since as it was observed the R245fa bubble has the smallest detachment volume and detachment time than the other two cases of Section 4 (Water/Air and Decane vapour/liquid). Therefore, it was more computationally efficient to perform 3D parametric numerical experiments for the case of refrigerant R245fa. The same uniform cell size is used as in the proposed axisymmetric simulation in the finer mesh region (32 cells per orifice diameter), while after the domain of main interest the mesh gradually coarsens, using two successively coarser domains. As in the axisymmetric case, a 3D parabolic inflow profile is used for the circular inlet boundary, with the maximum value of velocity being at the centre and radically decreasing to zero at the circular edge. For the bottom and circumferential solid boundaries a wall boundary condition is applied, while the top boundary of the domain represents the outlet boundary.

For the proposed, parametric, numerical investigation the same initial conditions with the axisymmetric case were used. The only thing that was varied between each numerical experiment, was the inclination angle of the gravity vector with respect to the bottom wall horizontal plane. A total of 9 simulations were performed, with the proposed inclination angle taking values from $\theta=90^\circ$ (gravity vector parallel to the vapor injection axis, as in the axisymmetric case of Section 4), up to $\theta=10^\circ$ with 10° increments. The results of the $\theta=90^\circ$ case were initially compared with the corresponding axisymmetric case, and it was found that the differences in the predictions of the bubble detachment characteristics were negligible (less than 1%).

Figure 15 depicts indicatively, the bubble growth and detachment characteristics for 3 of the 9 in total simulated cases. For each of the illustrated inclination angles of the gravity vector, the time instance of bubble detachment as well as a time instance 4 msec before and 4 msec after the bubble detachment are shown. The 0.5 volume fraction iso-surface, together with the velocity magnitude contours as well as the velocity vector field, in a vertical center section of the computational domain, are illustrated for each time instance.

Comparing the bubble growth and detachment process of the $\theta=90^\circ$ case (Figure 15a) with the other cases that the gravity vector inclination angle to the horizontal plane successively decreases (Figures 15b and 15c), some worth mentioning macroscopic conclusions can be drawn. Generally, as it was also discussed in the previous sections of the present paper, the bubble growth and detachment process constitutes a quite complex hydrodynamic phenomenon, that in the quasi-static growth regime, is governed mainly by the interactions between the buoyancy force and the surface tension force at the interface between the gaseous and liquid phases. In the first case ($\theta=90^\circ$) this hydrodynamic complexity is significantly reduced, as the interface evolution remains axisymmetric both before and after the time of bubble detachment. This simplicity in the process mainly arises from the fact that the governing force balance in all stages of interface evolution, consists of parallel forces acting on the bubble, in the direction of the gravitational acceleration. On the contrary, as the gravity vector direction gradually deviates from being parallel to the orifice longitudinal axis, the proposed axisymmetry is gradually lost, and the bubble shape as well as the surrounding flow field becomes three-dimensional. This happens since the force balance is now more complicated, as the buoyancy force

acts in each case in a different direction and the surface tension forces act along a different interfacial shape. From the hydrodynamics point of view, it is evident that the initially symmetric vortices (recirculation regions) in the flow domain ($\theta=90^\circ$), gradually become asymmetric with the left side vortex gradually reducing and the right side vortex gradually increasing in size ($\theta=50^\circ$) and finally predominating ($\theta=10^\circ$). This corresponding gradual decrease and increase in the initially symmetric and equal in size recirculation regions, deflect the growing bubble to the direction of the smaller vortex, leading also to a different initial direction and shape of the detaching bubble.

But in order to examine the influence on the bubble growth and detachment characteristics from a more quantitative point of view, graphs of the resulting bubble detachment times and volumes, with respect to the gravity vector inclination angle are illustrated in the diagrams of Figure 16a and 16b, respectively. As it can be observed from the graphs of Figure 15, both the bubble detachment time as well as the bubble detachment volume, decrease, as the gravity vector direction gradually deviates from being parallel to the vapor injection axis ($\theta=90^\circ$) and tending to become normal to the orifice axis ($\theta=10^\circ$). One can observe that the rate of decrease of both the bubble detachment time and volume is non-linear. For gravity vector inclination angles from $\theta=90^\circ$ up to $\theta=80^\circ$, a relatively small rate of decrease is observed, which then gradually increases up to an almost constant rate from $\theta=70^\circ$ up to $\theta=30^\circ$. Finally, at the last range of the examined inclination angles ($\theta=30^\circ$ up to $\theta=10^\circ$) a gradual decrease in the rates of decrease is evident.

From all the above observations it can be concluded that the underlying hydrodynamics in adiabatic bubble growth and detachment, are also strongly dependent on the gravity vector inclination angle with respect to the injection orifice longitudinal axis. However, it should be mentioned that since the numerical model of the present investigation has been validated against experimental data where the vapor injection axis is parallel to the gravitational vector, further validation with potential future, literature available experimental data where the vapor injection axis is inclined with respect to the gravitational vector, must be conducted for future investigations.

6. CONCLUSIONS

In the present paper, the algebraic VOF (Volume of Fluid) based interface capturing approach that is already implemented in the CFD ToolBox of OpenFOAM® (v.2.2.1), is adopted and further improved for the conduction of axisymmetric and 3D numerical experiments on adiabatic bubble growth dynamics. The main goal was the identification of the exact quantitative effect of fundamental parameters on the bubble growth dynamics, focusing on the detachment characteristics of isolated gas/vapour bubbles (from inception to departure), emanating quasi-statically from orifices submerged in isothermal liquid pools. Prior to the main applications the adopted VOF model is accordingly modified and improved, in order to account for the adequate reduction of the spurious velocities that are formed in the vicinity of the interface, leading to unphysical results. The predictions of the improved model, are quantitatively validated against literature available experimental data, showing an excellent degree of convergence. The optimised and validated version of the numerical model is then applied for the conduction of two wide series of numerical simulations. The first series, quantitatively explores the parametric effects of a wide range of liquid phase properties (surface tension, density and dynamic viscosity), for five different gravity levels that correspond to the main planets in the solar system, through 2D axisymmetric simulations. In the second series, the quantitative effect of the gravity vector direction inclination with respect to the bubble injection axis is investigated for the gravity level of Earth, utilising 3D numerical situations. From the overall analysis and discussion of the results the following important conclusions can be withdrawn:

- Among the examined fundamental controlling parameters, it is shown that the gravitational acceleration, the surface tension as well as the liquid phase density, influence significantly the bubble detachment

characteristics. On the contrary, in comparison to the influence of the aforementioned controlling parameters, the variation of the liquid phase dynamic viscosity has a minimal effect both in the equivalent bubble detachment diameter as well as in the bubble detachment time.

- In all of the considered gravity levels, the bubble detachment diameter as well as the bubble detachment time follow a linear increase with the increase of the surface tension. However, as the gravity level successively reduces to significantly lower values than the gravity level of the Earth, apart from the expected higher values in the bubble detachment characteristics, a successive increase in the slope of the resulted linear trend is evident.
- Both the bubble detachment diameter as well as the bubble detachment time, decrease following a power law with respect to the corresponding increase of the liquid phase density. Again, with successively lower gravity levels, the bubble detachment characteristics show significantly higher values and their rate of increase with respect to the corresponding decrease of the liquid phase density becomes successively higher.
- Regarding the effect of the liquid phase dynamic viscosity, generally a negligible linear increase of the bubble detachment characteristics is observed, with respect to the corresponding significant increase of the proposed fluid property. However, it is important that for the lowest of the considered gravity levels (Pluto), which is significantly lower than the gravity level of Earth, and for the lowest value range of the examined dynamic viscosities, both the bubble detachment diameter as well as the bubble detachment time present a quite significant increase that is not present for higher gravitational accelerations.
- It is characteristic that, the influence of all of the examined controlling parameters, is higher in the bubble detachment time in comparison to the bubble detachment diameter.
- For gravity levels close to the Earth's gravity, the relative change of the bubble detachment characteristics with respect to the variation of the examined fluid properties, is almost the same. However, as the gravity level significantly reduces the relative change of the bubble detachment characteristics is quite higher than the corresponding relative change in the gravity level of Earth.
- A correction to an existing theoretical correlation that results from a simplified force balance is proposed, leading to a relationship that for the examined ranges of Eötvös numbers it can be safely applied for the prediction of the bubble detachment diameter. A similar correlation is also proposed for the prediction of the bubble detachment time. However these correlations are limited to low viscosity fluids.
- Apart from the fluid properties and the magnitude of the gravitational acceleration, it is shown that the bubble detachment characteristics are also strongly dependent on the gravity vector inclination angle with respect to the injection orifice longitudinal axis. Both the bubble detachment volume as well as the bubble detachment time, reduce significantly as the gravity vector direction gradually deviates from being parallel to the vapour injection orifice, following a non-linear decrease.

Summarizing, the present investigation adds significantly to the existing knowledge on bubble growth and detachment, from submerged orifices into isothermal liquid pools, since a comprehensive examination of the effect of fundamental

controlling parameters on the bubble detachment characteristics is conducted, identifying their exact quantitative influence on the bubble detachment diameter and time as well as their relative importance. Furthermore, from dimensionless analysis on the overall numerical results two correlations are derived, that for the examined range of Eötvös number, are able to predict the equivalent bubble detachment diameter and the bubble detachment time, respectively. Finally, it can be said that the use of the improved VOF-based interface capturing approach that is presented, validated and applied in the present investigation, constitutes a quite promising tool for the simulation of adiabatic bubble growth and detachment processes, providing great insight regarding the complex underlined physics and hydrodynamics, of such two-phase flow phenomena of significant interest to real technological applications.

ACKNOWLEDGMENT

The results presented in the present paper, constitute the first part of a more wider research work, which is related to the development of a VOF-based flow boiling model, able to predict the bubble detachment characteristics in cases of diesel fuel flow boiling within injector nozzles, and it has received funding from the People Programme (IAPP Marie Curie Actions) of the European Union's Seventh Framework Programme FP7/2007-2013/ under REA grant agreement n. 324313. The authors would also like to acknowledge the contribution of the super-computing facilities of CINECA, in Bologna (Italy), for the conduction of the large number of numerical simulations of the present investigation, in a relatively short time.

REFERENCES

- Albadawi, A., Delauré, Y., Donoghue, D.B., Robinson, A., Murray, D.B., 2012. Numerical investigation of volume of fluid and level set interface capturing methods for bubble growth and detachment. *J. Phys. Conf. Ser.* 395, 012166. doi:10.1088/1742-6596/395/1/012166.
- Albadawi, a., Donoghue, D.B., Robinson, a. J., Murray, D.B., Delauré, Y.M.C., 2013a. Influence of surface tension implementation in Volume of Fluid and coupled Volume of Fluid with Level Set methods for bubble growth and detachment. *Int. J. Multiph. Flow* 53, 11–28. doi:10.1016/j.ijmultiphaseflow.2013.01.005.
- Albadawi, A., Donoghue, D.B., Robinson, A.J., Murray, D.B., Delauré, Y.M.C., 2013b. On the analysis of bubble growth and detachment at low Capillary and Bond numbers using Volume of Fluid and Level Set methods. *Chem. Eng. Sci.* 90, 77–91. doi:10.1016/j.ces.2012.12.004.
- Benzing, R.J., Myers, J.E., 1955. Low Frequency Bubble Formation at Horizontal Circular Orifices. *Ind. Eng. Chem.* 47, 2087–2090. doi:10.1021/ie50550a022.
- Brackbill, J., Kothe, D., Zemach, C., 1992. A continuum method for modeling surface tension. *J. Comput. Phys.* 100, 335–354. doi:10.1016/0021-9991(92)90240-Y.
- Byakova, A., Gnyloskurenko, S., Nakamura, T., Raychenko, O., 2003. Influence of wetting conditions on bubble formation at orifice in an inviscid liquid. *Colloids Surfaces A Physicochem. Eng. Asp.* 229, 19–32. doi:10.1016/j.colsurfa.2003.08.009.
- Chakraborty, I., Biswas, G., Ghoshdastidar, P.S., 2011. Bubble generation in quiescent and co-flowing liquids. *Int. J. Heat Mass Transf.* 54, 4673–4688. doi:10.1016/j.ijheatmasstransfer.2011.06.010.
- Chakraborty, I., Ray, B., Biswas, G., 2009. Computational investigation on bubble detachment from submerged orifice in quiescent liquid under normal and reduced gravity. *Phys. Fluids* 21, 062103. doi:10.1063/1.3152437.
- Das, A.K., Das, P.K., 2009. Bubble evolution through submerged orifice using smoothed particle hydrodynamics: Basic formulation and model validation. *Chem. Eng. Sci.* 64, 2281–2290. doi:10.1016/j.ces.2009.01.053.
- Das, A., Das, P., 2013. Bubble evolution and necking at a submerged orifice for the complete range of orifice tilt. *AIChE J.* 59. doi:10.1002/aic.

- Davidson, J., Schuler, B., 1960. Bubble formation at an orifice in a viscous liquid, *Trans. Amer. Inst. Chem. Eng.* 38, 144–154.
- Deshpande, S.S., Anumolu, L., Trujillo, M.F., 2012. Evaluating the performance of the two-phase flow solver interFoam. *Comput. Sci. Discov.* 5, 014016. doi:10.1088/1749-4699/5/1/014016.
- Di Bari, S., Lakehal, D., Robinson, A.J., 2013. A numerical study of quasi-static gas injected bubble growth: Some aspects of gravity. *Int. J. Heat Mass Transf.* 64, 468–482. doi:10.1016/j.ijheatmasstransfer.2013.04.002.
- Di Bari, S., Robinson, A.J., 2013a. Experimental study of gas injected bubble growth from submerged orifices. *Exp. Therm. Fluid Sci.* 44, 124–137. doi:10.1016/j.expthermflusci.2012.06.005.
- Di Bari, S., Robinson, A.J., 2013b. Adiabatic bubble growth in uniform DC electric fields. *Exp. Therm. Fluid Sci.* 44, 114–123. doi:10.1016/j.expthermflusci.2012.06.004.
- Di Marco, P., Grassi, W., Memoli, G., 2003. Influence of electric field on single gas-bubble growth and detachment in microgravity. *Int. J. ...* 29, 559–578. doi:10.1016/S0301-9322(03)00030-2.
- Di Marco, P., 2005. Birth, Life and Death of Gas Bubbles Rising in a Stagnant Liquid. *Heat Technol.* 23, 17–26.
- Di Marco, P., Morganti, N., Saccone, G., 2013. Growth and detachment of gas bubbles from an inclined surface, in: 31st UIT Heat Transfer Conference. Como.
- Dietrich, N., Mayoufi, N., Poncin, S., Li, H.Z., 2013. Experimental investigation of bubble and drop formation at submerged orifices. *Chem. Pap.* 67, 313–325.
- Forrester, S.E., Rielly, C.D., 1998. Bubble formation from cylindrical, flat and concave sections exposed to a strong liquid cross-flow. *Chem. Eng. Sci.* 53, 1517–1527. doi:10.1016/S0009-2509(98)00019-0.
- Frank, X., Funfschilling, D., Midoux, N., Li, H.Z., 2005. Bubbles in a viscous liquid: lattice Boltzmann simulation and experimental validation. *J. Fluid Mech.* 546, 113–122. doi:10.1017/S0022112005007135.
- Gerlach, D., Alleborn, N., Buwa, V., Durst, F., 2007. Numerical simulation of periodic bubble formation at a submerged orifice with constant gas flow rate. *Chem. Eng. Sci.* 62, 2109–2125. doi:10.1016/j.ces.2006.12.061.
- Gerlach, D., Biswas, G., Durst, F., Kolobaric, V., 2005. Quasi-static bubble formation on submerged orifices. *Int. J. Heat Mass Transf.* 48, 425–438. doi:10.1016/j.ijheatmasstransfer.2004.09.002.
- Hoang, D.A., van Steijn, V., Portela, L.M., Kreutzer, M.T., Kleijn, C.R., 2013. Benchmark numerical simulations of segmented two-phase flows in microchannels using the Volume of Fluid method. *Comput. Fluids* 86, 28–36. doi:10.1016/j.compfluid.2013.06.024.
- Hua, J., Lou, J., 2007. Numerical simulation of bubble rising in viscous liquid. *J. Comput. Phys.* 222, 769–795. doi:10.1016/j.jcp.2006.08.008.
- Kasimsetty, S.K., Subrahmani, A., Manglik, R.M., Jog, M.A., 2007. Theoretical Modeling and Experimental Measurements of Single Bubble Dynamics from a Submerged Orifice in a Liquid Pool, in: ASME-JSME Thermal Engineering Summer Heat Transfer Conference. Vancouver, pp. 9–17. doi:10.1115/HT2007-32088.
- Kim, I., Kamotani, Y., Ostrach, S., 1994. Modeling bubble and drop formation in flowing liquids in microgravity. *AIChE J.* 40, 19–28. doi:10.1002/aic.690400105.
- Kulkarni, A.A., Joshi, J.B., 2005. Bubble Formation and Bubble Rise Velocity in Gas–Liquid Systems:□ A Review. *Ind. Eng. Chem. Res.* 44, 5873–5931. doi:10.1021/ie049131p.
- Kumar, R., Kuloor, N.K., 1970. *Advances in Chemical Engineering Volume 8, Advances in Chemical Engineering, Advances in Chemical Engineering.* Elsevier. doi:10.1016/S0065-2377(08)60186-6.
- Lee, S.-L., Tien, W.-B., 2009. Growth and detachment of carbon dioxide bubbles on a horizontal porous surface with a uniform mass injection. *Int. J. Heat Mass Transf.* 52, 3000–3008. doi:10.1016/j.ijheatmasstransfer.2009.01.040.

- Marshall, S.H., Chudacek, M.W., Bagster, D.F., 1993. A model for bubble formation from an orifice with liquid cross-flow. *Chem. Eng. Sci.* 48, 2049–2059. doi:10.1016/0009-2509(93)80081-Z.
- McCann, D.J., Prince, R.G.H., 1969. Bubble formation and weeping at a submerged orifice. *Chem. Eng. Sci.* 24, 801–814. doi:10.1016/0009-2509(69)85001-3.
- Oguz, H., Prosperetti, A., 1993. Dynamics of bubble growth and detachment from a needle. *J. Fluid Mech.* 257, 111–145.
- OpenFOAM 2013. The OpenSource CFD Toolbox, User Guide, Version 2.2.1.
- Pamperin, O., Rath, H.-J., 1995. Influence of buoyancy on bubble formation at submerged orifices. *Chem. Eng. Sci.* 50, 3009–3024. doi:10.1016/0009-2509(95)00140-Z.
- Pianet, G., Vincent, S., Leboi, J., Caltagirone, J.P., Anderhuber, M., 2010. Simulating compressible gas bubbles with a smooth volume tracking 1-Fluid method. *Int. J. Multiph. Flow* 36, 273–283. doi:10.1016/j.ijmultiphaseflow.2009.12.002.
- Quan, S., Hua, J., 2008. Numerical studies of bubble necking in viscous liquids. *Phys. Rev. E* 77, 066303. doi:10.1103/PhysRevE.77.066303.
- Scardovelli, R., Zaleski, S., 1999. Direct Numerical Simulation of Free-Surface and Interfacial Flow. *Annu. Rev. Fluid Mech.* 31, 567–603. doi:10.1146/annurev.fluid.31.1.567.
- Subramani, A., Jog, M.A., Manglik, R.M., 2007. Experimental Study of Single-Bubble Dynamics in Isothermal Liquid Pools: Effects of Fluid Properties, Orifice Diameter and Flow Rate, in: *ASME 2007 International Mechanical Engineering Congress and Exposition*. pp. 1639–1645. doi:10.1115/IMECE2007-43442.
- Swope, R., 1971. Single bubble formation at orifices submerged in viscous liquids. *Can. J. Chem. Eng.* 49, 169–174. doi:10.1002/cjce.5450490201.
- Tsuge, H., Terasaka, K., Koshida, W., Matsue, H., 1997. Bubble formation at submerged nozzles for small gas flow rate under low gravity. *Chem. Eng. Sci.* 52, 3415–3420. doi:10.1016/S0009-2509(97)00159-0.
- Tsuge, H., Tezuka, Y., Mitsudani, M., 2006. Bubble formation mechanism from downward nozzle—Effect of nozzle shape and operating parameters. *Chem. Eng. Sci.* 61, 3290–3298. doi:10.1016/j.ces.2005.12.002.
- Ubbink, O., 1997. Numerical prediction of two fluid systems with sharp interfaces. Imperial College of Science, Technology & Medicine.
- Unverdi, S.O., Tryggvason, G., 1992. A front-tracking method for viscous, incompressible, multi-fluid flows. *J. Comput. Phys.* 100, 25–37. doi:10.1016/0021-9991(92)90307-K.
- Walters, J., Davidson, J., 1962. The initial motion of a gas bubble formed in an inviscid liquid Part 1. The two-dimensional bubble. *J. Fluid Mech.* 12, 408–417.
- Walters, J., Davidson, J., 1963. The initial motion of a gas bubble formed in an inviscid liquid Part 2. The three-dimensional bubble and the toroidal bubble. *J. Fluid Mech.* 17, 321–336.
- Zhang, L., Shoji, M., 2001. Aperiodic bubble formation from a submerged orifice 56, 5371–5381.
- Zhu, X., Liao, Q., Wang, H., Bao, L.J., Xie, J., Lin, C.X., 2010. Experimental Study of Bubble Growth and Departure at the Tip of Capillary Tubes with Various Wettabilities in a Stagnant Liquid. *J. Supercond. Nov. Magn.* 23, 1141–1145. doi:10.1007/s10948-010-0723-y.

Table 1 Initial conditions for the numerical simulations (Validation Cases 1 and 2).

Parameter	Symbol	Values		Units
		(Case1)	(Case2)	
Liquid Dynamic Viscosity	μ_l	0.001	0.0014	kg/m s
Gas Dynamic Viscosity	μ_g	1.79×10^{-5}	1.824×10^{-5}	kg/m s
Liquid Density	ρ_l	998.2	998.12	kg/m ³
Gas Density	ρ_g	1.225	1.188	kg/m ³
Surface Tension Coeff.	σ	0.073	0.07273	N/m
Orifice radius	R_c	0.8	1.35	mm
Gas Injection Flow Rate	Q	4.17×10^{-8}	1.67×10^{-8}	m ³ /s

Table 2 Comparison of Bubble detachment characteristics between experimental and numerical results from three different VOF-based CFD solvers.

METHOD	REFERENCE	t_{det} (sec)	Et_{det} (%)	V_{det} (mm ³)	EV_{det} (%)
Experimental	Albadawi et al. (2013b)	0.684	0	29.699	0
VOF(Ansys Fluent)	Albadawi et al. (2013b)	0.834	21.9	35.804	20.56
VOF (OpenFOAM) Original	Albadawi et al. (2013b)	0.429	-37.2	21.022	29.22
VOF (OpenFOAM) Smooth	Present work	0.617	-9.8	26.769	-10.9

Table 3 Fluid properties for the simulated cases of R245fa vapour/liquid and Decane vapour/liquid.

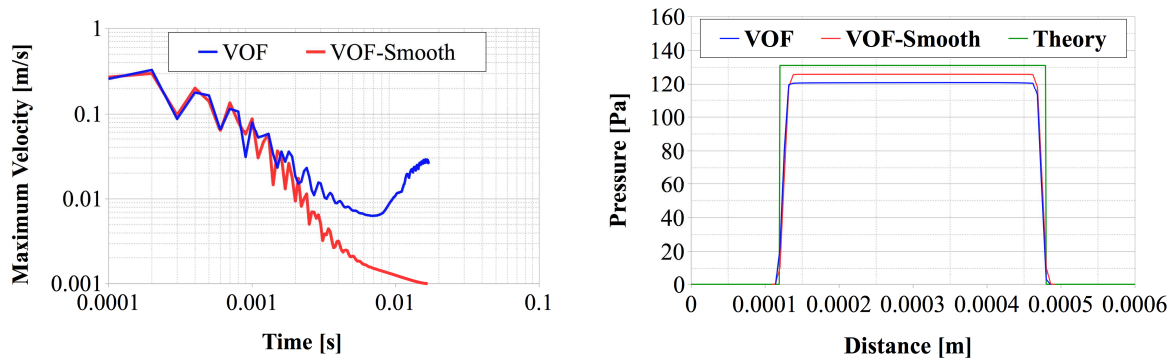
Parameter	Symbol	Case	Value	Units
Liquid Dynamic Viscosity	μ_l	R245fa	4.64×10^{-4}	kg/m s
		Decane	0.63	
Gas Dynamic Viscosity	μ_g	R245fa	9.96×10^{-6}	kg/m s
		Decane	3.09×10^{-5}	
Liquid Density	ρ_l	R245fa	1364.90	kg/m ³
		Decane	730.26	
Gas Density	ρ_g	R245fa	5.96	kg/m ³
		Decane	5.91	
Surface Tension Coeff.	σ	R245fa	0.015	N/m
		Decane	0.025	

Table 4 Initial conditions for the base case and overall parameter variation.

Parameter	Symbol	Value	Units
Liquid Dynamic Viscosity	μ_l	4.64×10^{-4}	kg/m s
Gas Dynamic Viscosity	μ_g	9.96×10^{-6}	kg/m s
Liquid Density	ρ_l	1364.90	kg/m ³
Gas Density	ρ_g	5.96	kg/m ³
Surface Tension Coeff.	σ	0.01531	N/m
Orifice radius	R_c	0.8	mm
Gas Injection Flow Rate	Q	150×10^{-3}	l/h
Liquid Density Variation	250, 500, 750, 100, 1500, 1600 [kg/m ³]		
Liquid Dynamic Viscosity Variation	0.0001, 0.00023, 0.0008, 0.0009, 0.001, 0.002 [kg/m s] (low viscosity range) 0.025, 0.050, 0.07, 0.10 [kg/m s] (high viscosity range)		
Surface Tension Variation	0.01, 0.02, 0.03, 0.04, 0.05, 0.06 [N/m]		
Gravitational Acceleration Variation	0.58 (Pluto), 3.71 (Mars, Mercury), 8.83 (Venus, Saturn, Uranus), 9.81 (Earth), 10.99 (Neptune) [m/s ²]		

Table 5 Maximum variation factors in the examined fluid properties and corresponding maximum change factors for the equivalent bubble detachment diameter and the bubble detachment time, in all of the considered gravity levels.

Parameter	Max. Variation factor					Max. D_{eq}/D_0 change factor					Max. $t_{det}U_0/D_0$ change factor				
	<i>Gravity Level (m/s²)</i>					<i>Gravity Level (m/s²)</i>					<i>Gravity Level (m/s²)</i>				
	<i>10.99</i>	<i>9.81</i>	<i>8.83</i>	<i>3.71</i>	<i>0.58</i>	<i>10.99</i>	<i>9.81</i>	<i>8.83</i>	<i>3.71</i>	<i>0.58</i>	<i>10.99</i>	<i>9.81</i>	<i>8.83</i>	<i>3.71</i>	<i>0.58</i>
σ	6	6	6	6	6	1.6	1.62	1.61	1.63	1.71	5.44	5.54	5.32	4.83	5.11
ρ_l	6.4	6.4	6.4	6.4	6.4	1.69	1.70	1.69	1.72	1.81	6.20	6.15	5.95	5.55	6.02
μ_l	1000	1000	1000	1000	1000	1.21	1.20	1.20	1.17	1.15	2.02	1.94	1.91	1.67	1.55



(a) (b)

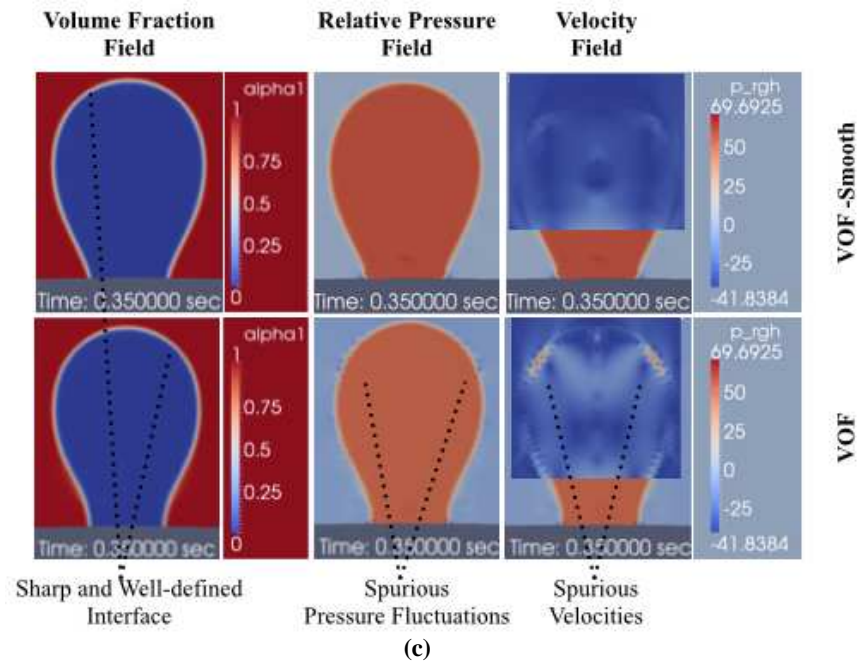


Fig. 1. Comparison of numerical predictions between the original and the modified VOF solver, for spurious currents dampening (Brackbill's test case), (b) for Laplace pressure difference (Brackbill's test case) and (c) for the case of a quasi-static air bubble growth in an isothermal water pool, from a submerged orifice.

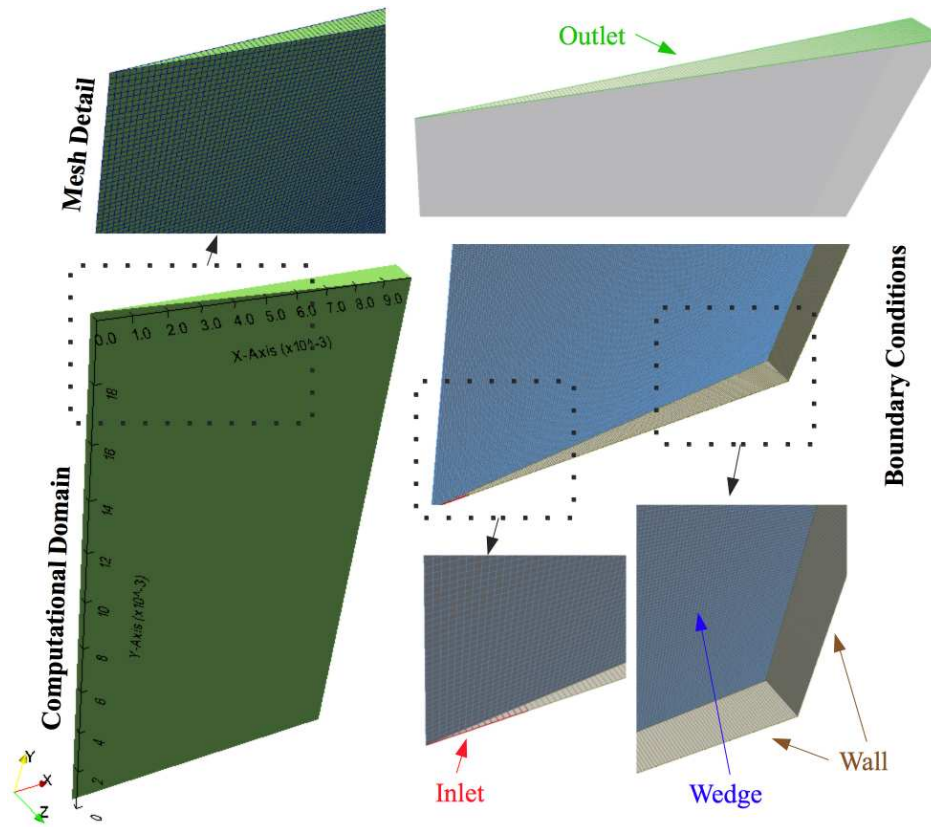


Fig. 2. Computational domain, mesh and boundary conditions.

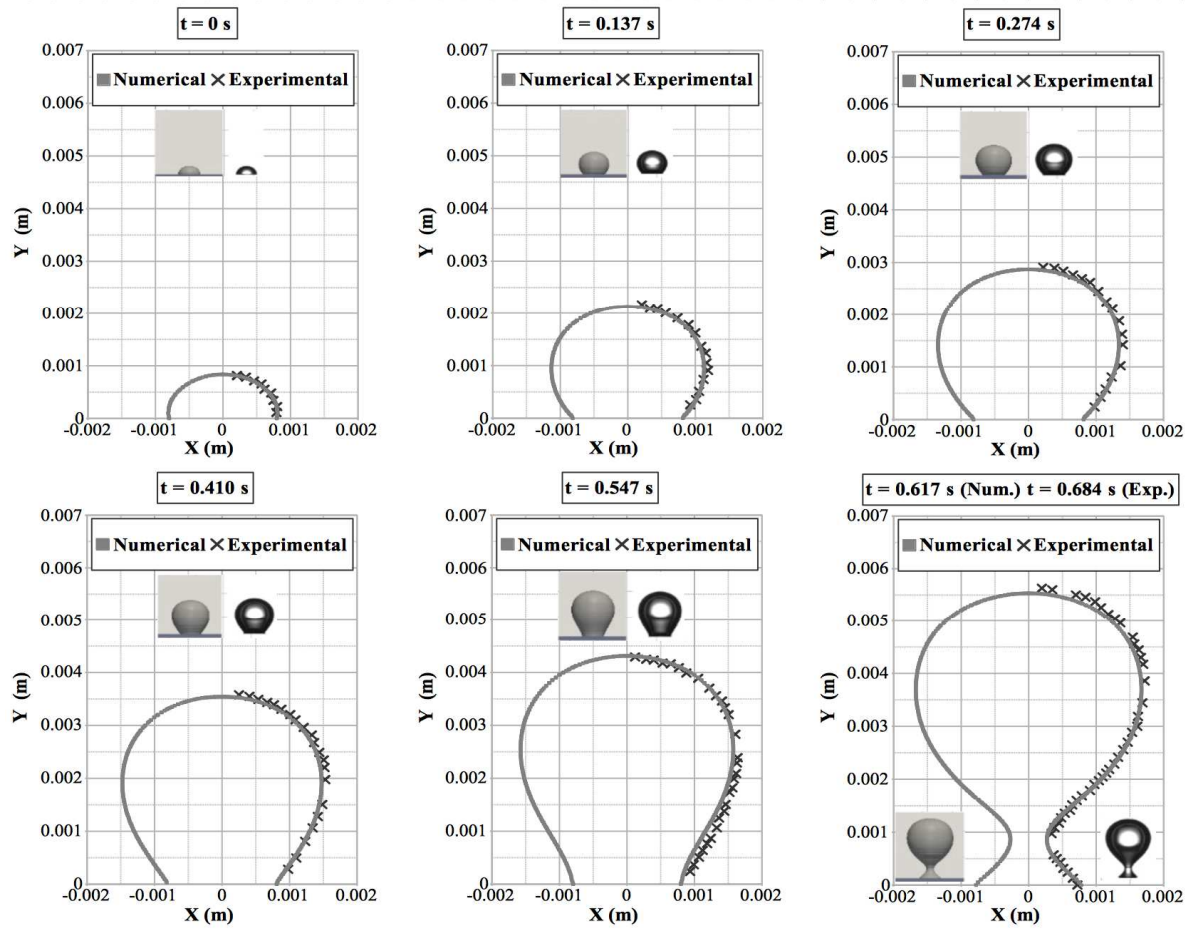


Fig. 3. Comparison of experimental (Albadawi et al., 2013b) and numerical (present study) interface position with time.

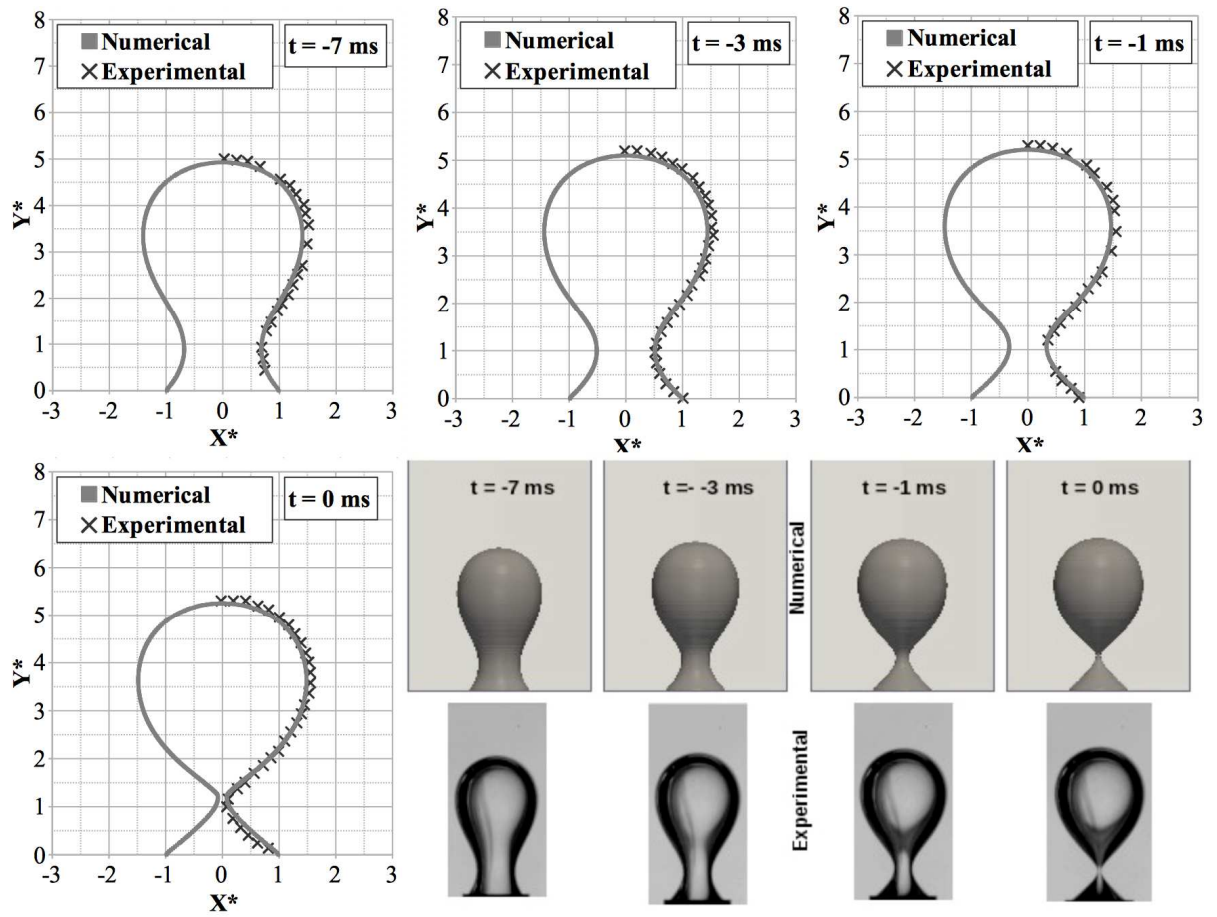


Fig. 4. Comparison of experimental (Quan and Hua, 2008) and numerical (present study) interface evolution of the generated bubble, before the time of detachment ($t = 0$ s).

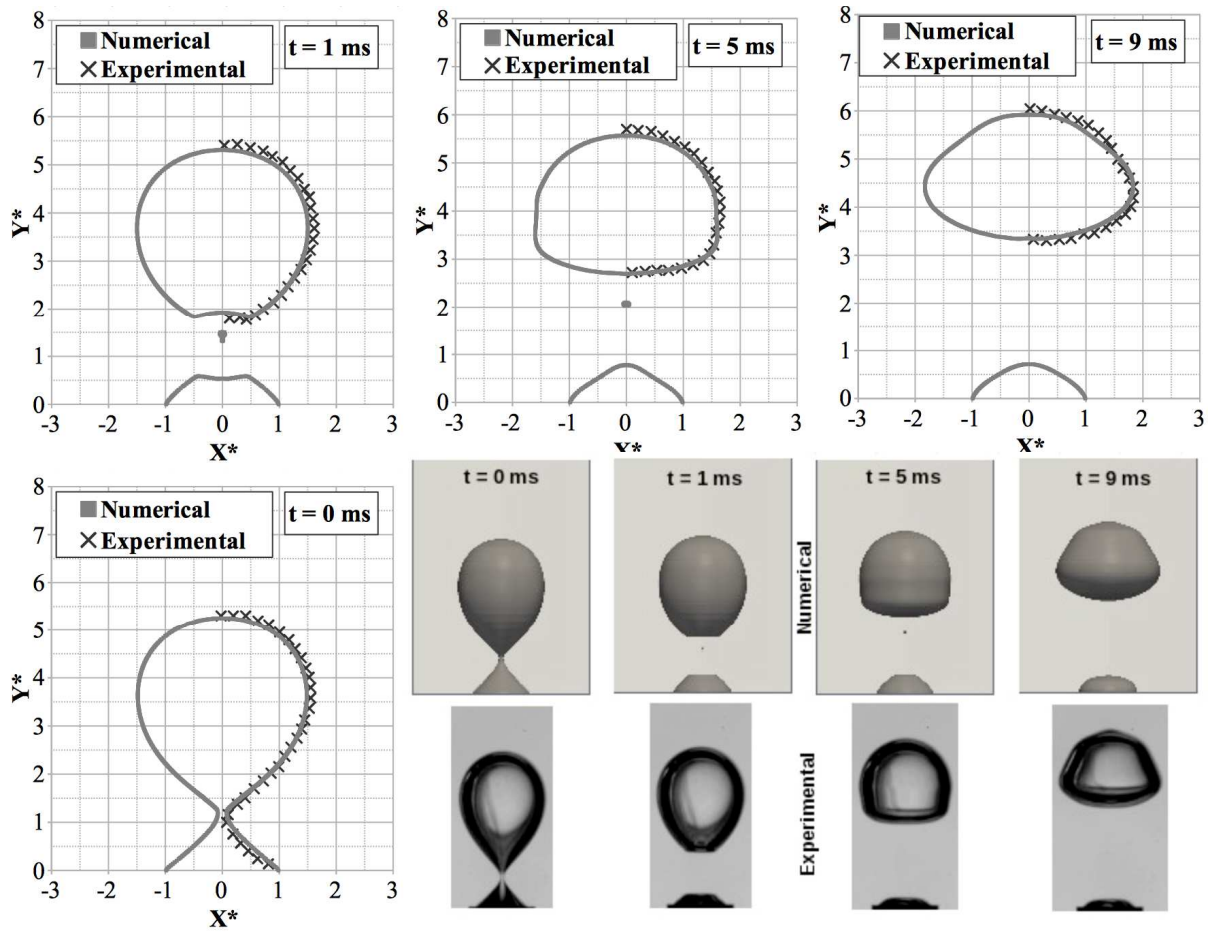


Fig. 5. Comparison of experimental (Quan and Hua, 2008) and numerical (present study) interface evolution of the generated bubble, after the time of detachment ($t = 0$ s).

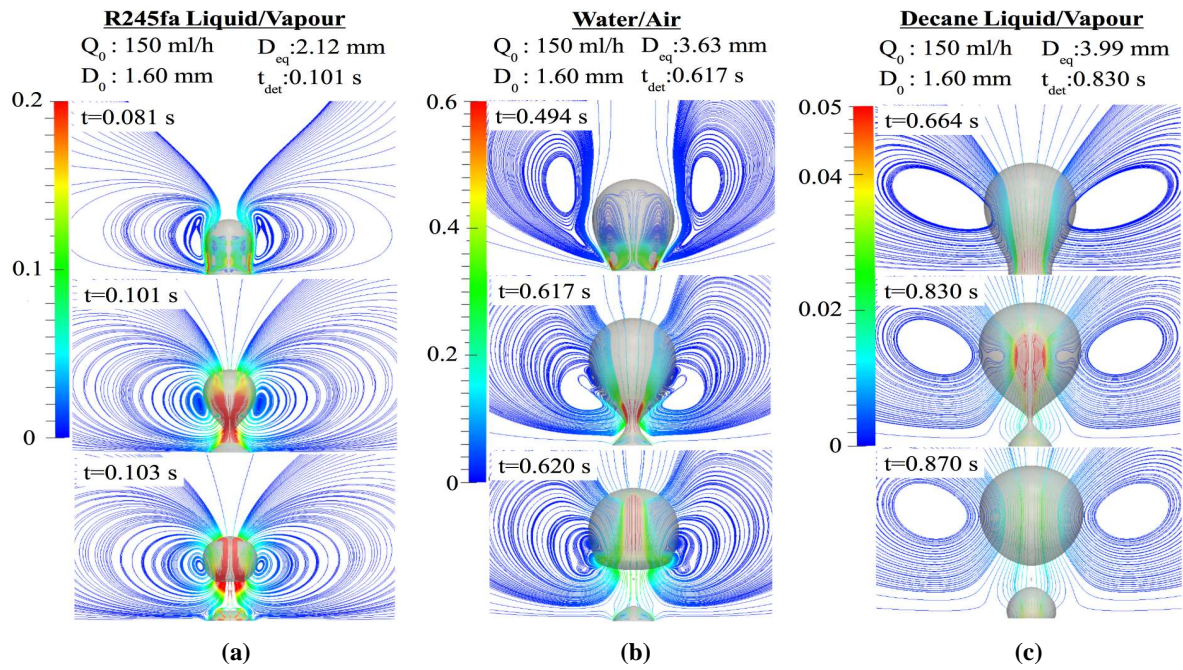


Fig. 6. Streamlines coloured by velocity magnitude during bubble growth and detachment for the three different two-phase flow cases: (a) R245fa vapour/liquid, (b) water and air and (c) Decane vapour/liquid.

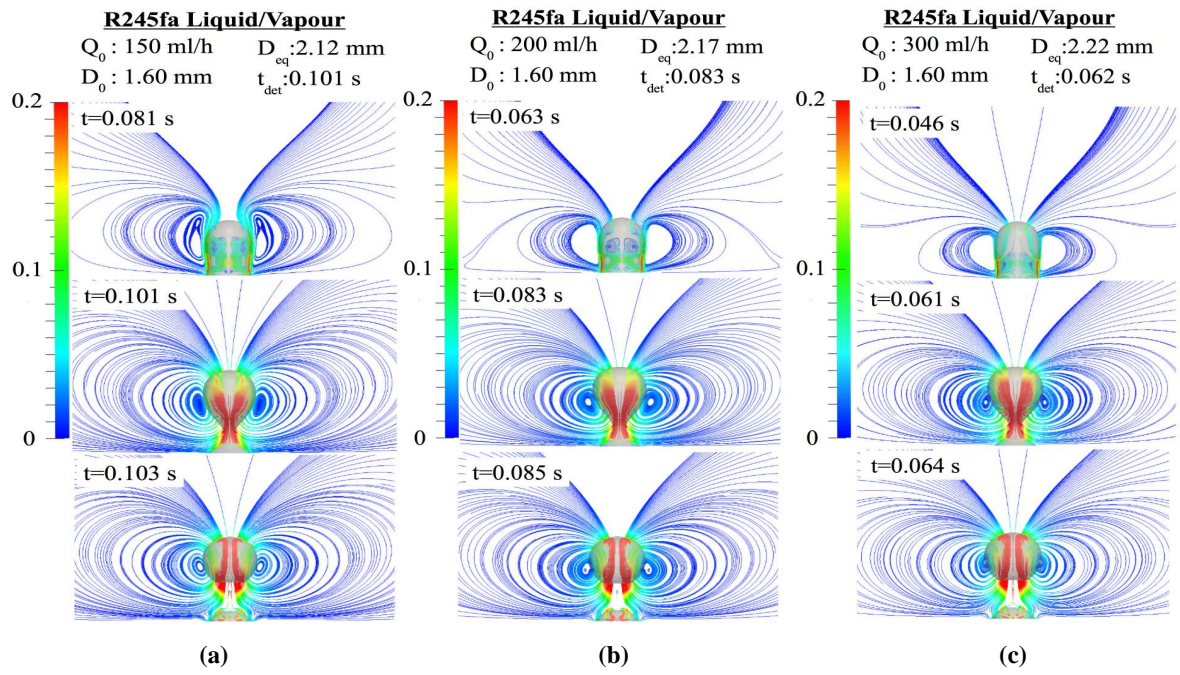


Fig. 7. Streamlines coloured by velocity magnitude during bubble growth and detachment for three different discharge values for the R245fa case: (a) 150 mlph, (b) 200mlph and (c) 300 mlph.

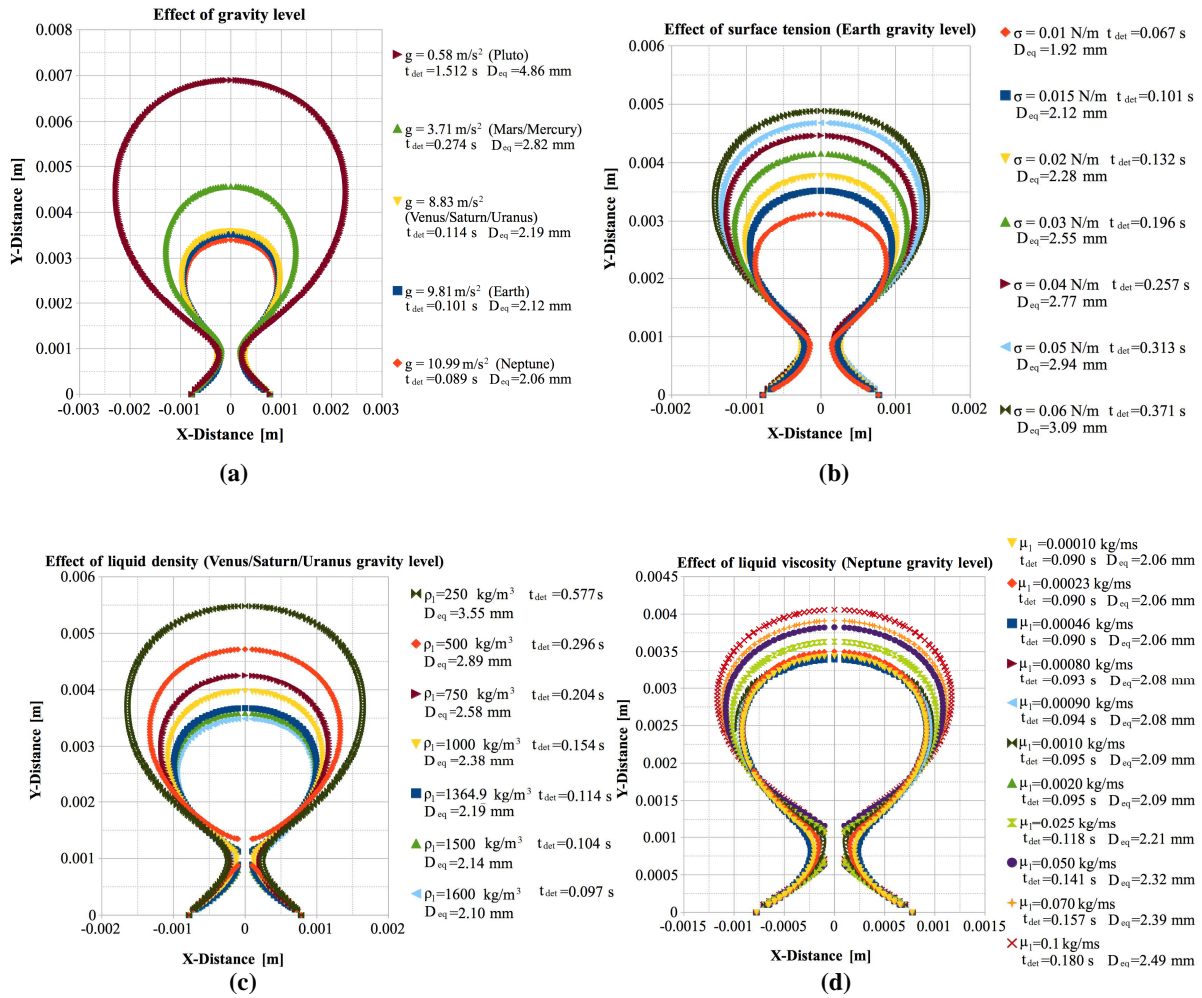


Fig. 8. Effect of the examined parameters variation in the generated bubble volume at the time instance just before its detachment from the orifice: a) gravity, b) surface tension (Earth gravity level), c) liquid phase density (Venus/Saturn/Uranus gravity level) and d) liquid phase viscosity (Neptune gravity level).

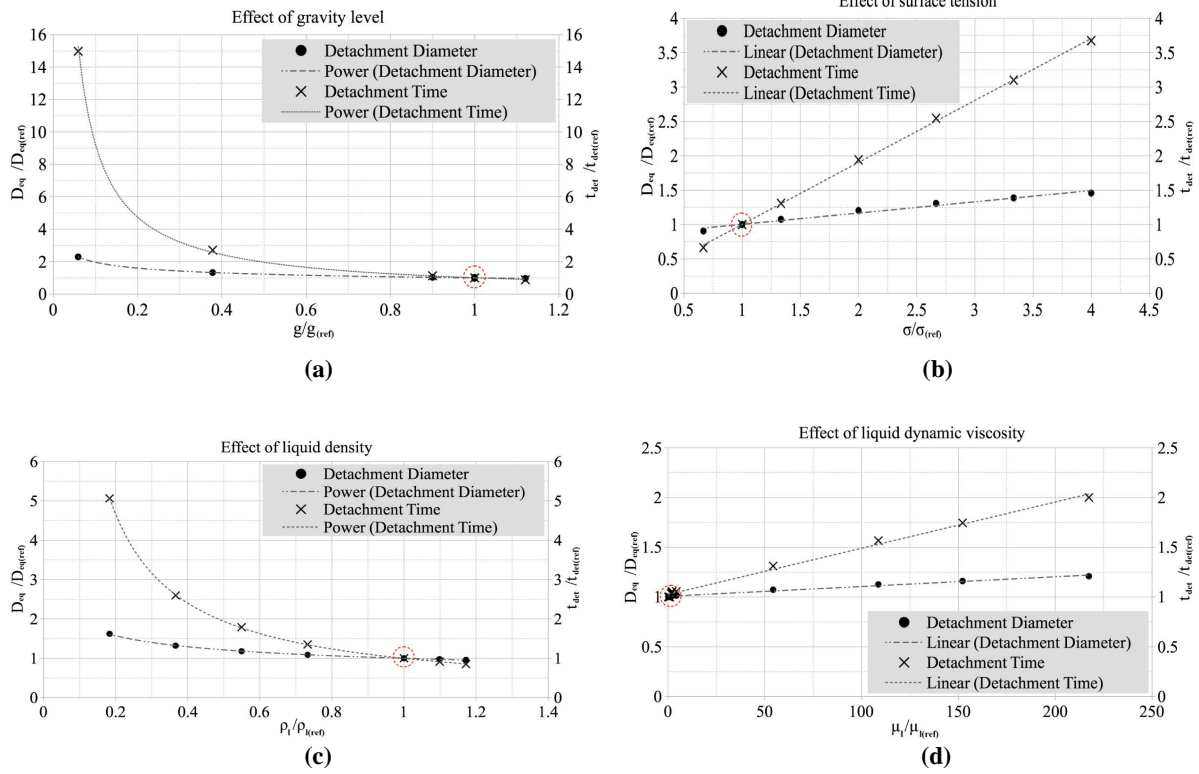


Fig. 9. Relative effect of examined parameters variation in the equivalent bubble detachment diameter and the bubble detachment time: a) gravity, b) surface tension, c) liquid phase density and d) liquid phase viscosity (all values are normalized by their corresponding reference values).

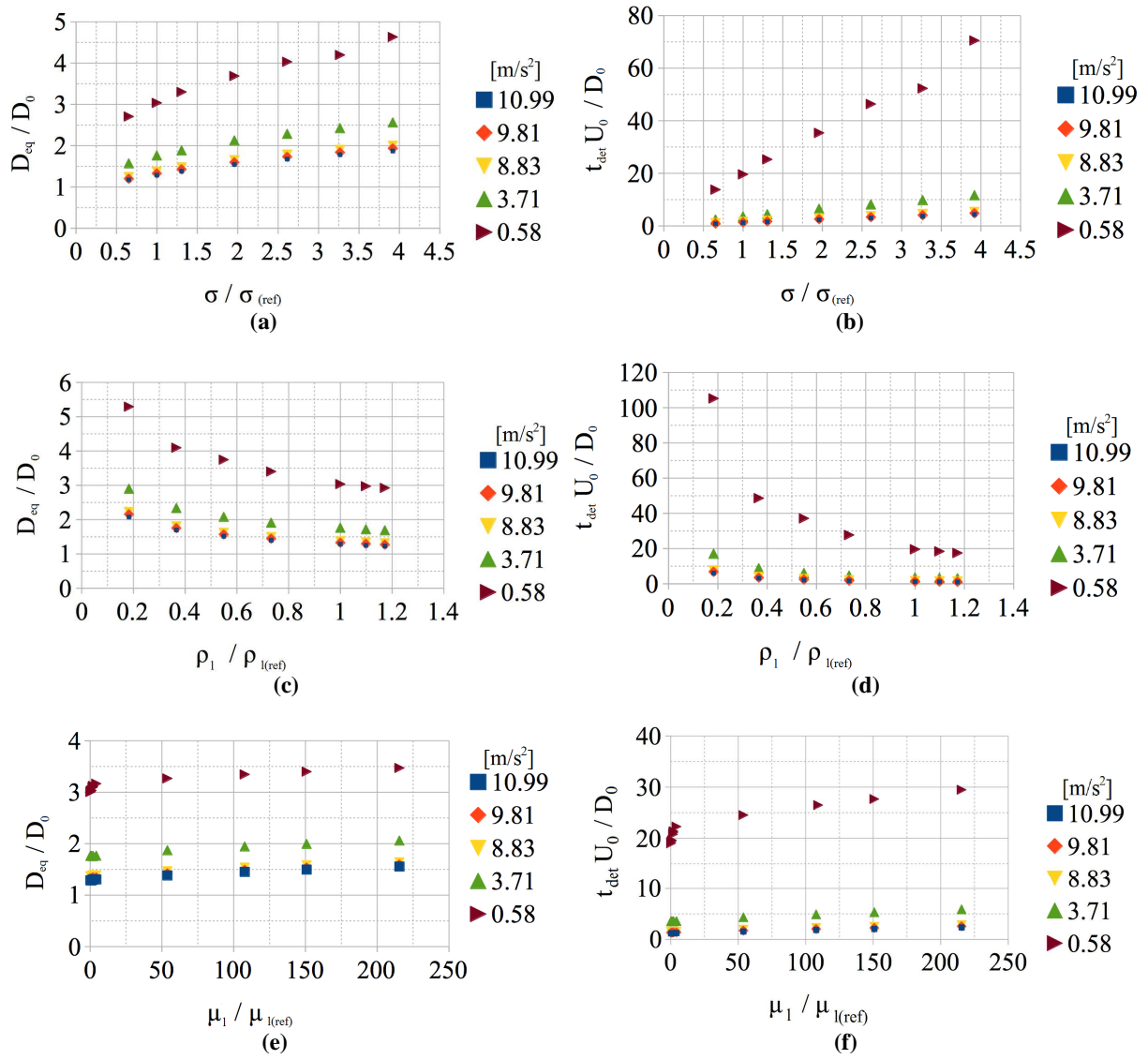


Fig. 10. Dimensionless equivalent bubble detachment diameter (left diagrams) and dimensionless detachment time (right diagrams) with respect to the varied parameters (normalised by the corresponding values of their reference simulation), for all the considered gravity levels.

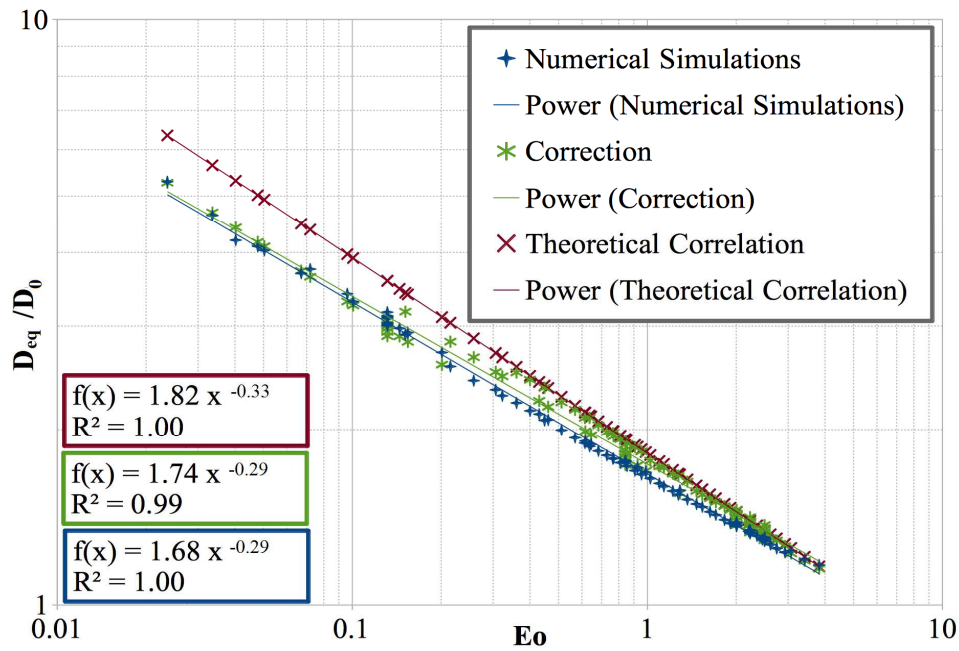


Fig. 11. Dimensionless equivalent bubble detachment diameter versus Eötvös number: numerical simulations excluding high viscosity runs (blue data points), theoretical correlation (brown data points) and suggested correction (green data points).

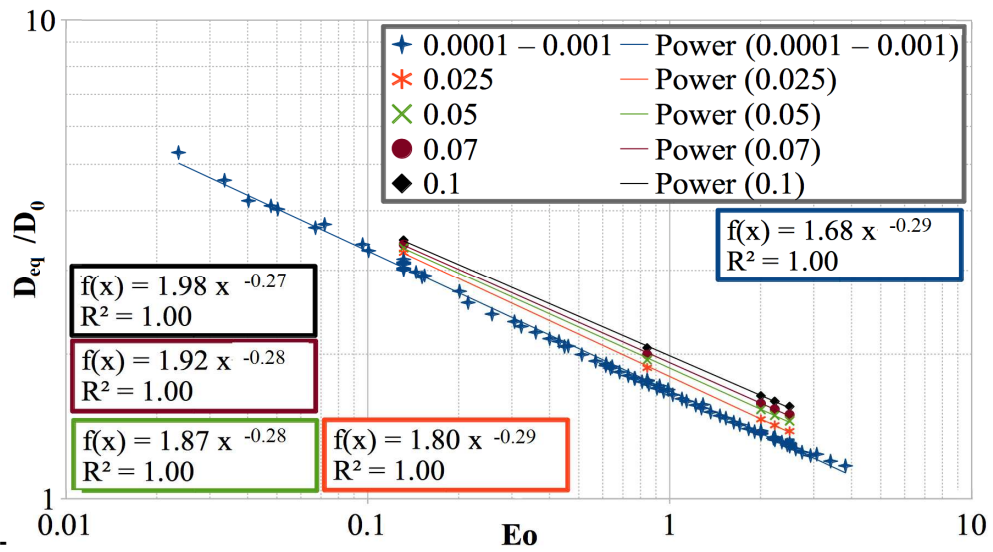


Fig. 12. Dimensionless equivalent bubble detachment diameter versus Eötvös number: numerical simulations excluding high viscosity runs (blue data points) and numerical simulations with liquid dynamic viscosity of 0.025 kg/m s (orange data points), 0.05 kg/m s (green data points), 0.07 kg/m s (brown data points) and 0.1 kg/m s (orange data points).

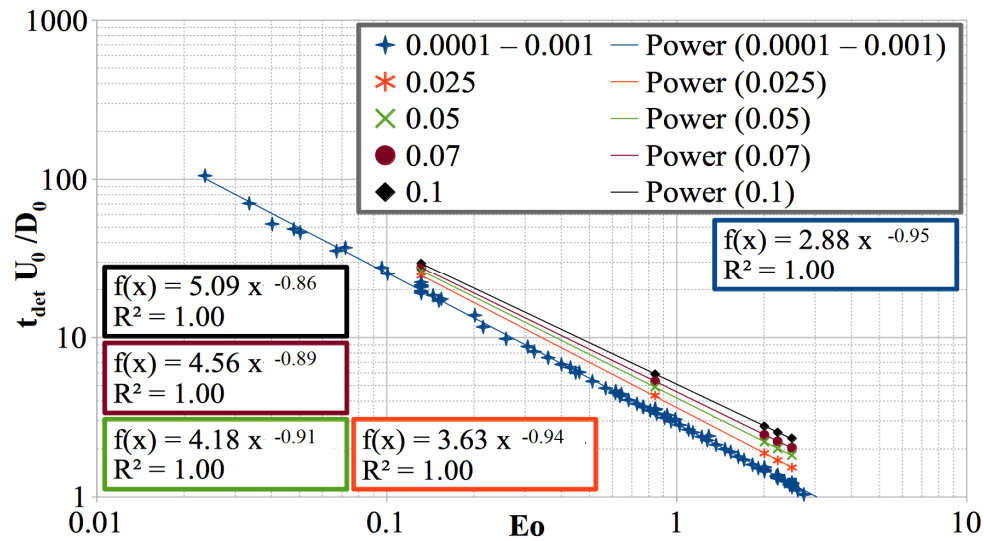


Fig. 13. Dimensionless bubble detachment time versus Eötvös number: numerical simulations excluding high viscosity runs (blue data points) and numerical simulations with liquid dynamic viscosity of 0.025 kg/m s (orange data points), 0.05 kg/m s (green data points), 0.07 kg/m s (brown data points) and 0.1 kg/m s (black data points).

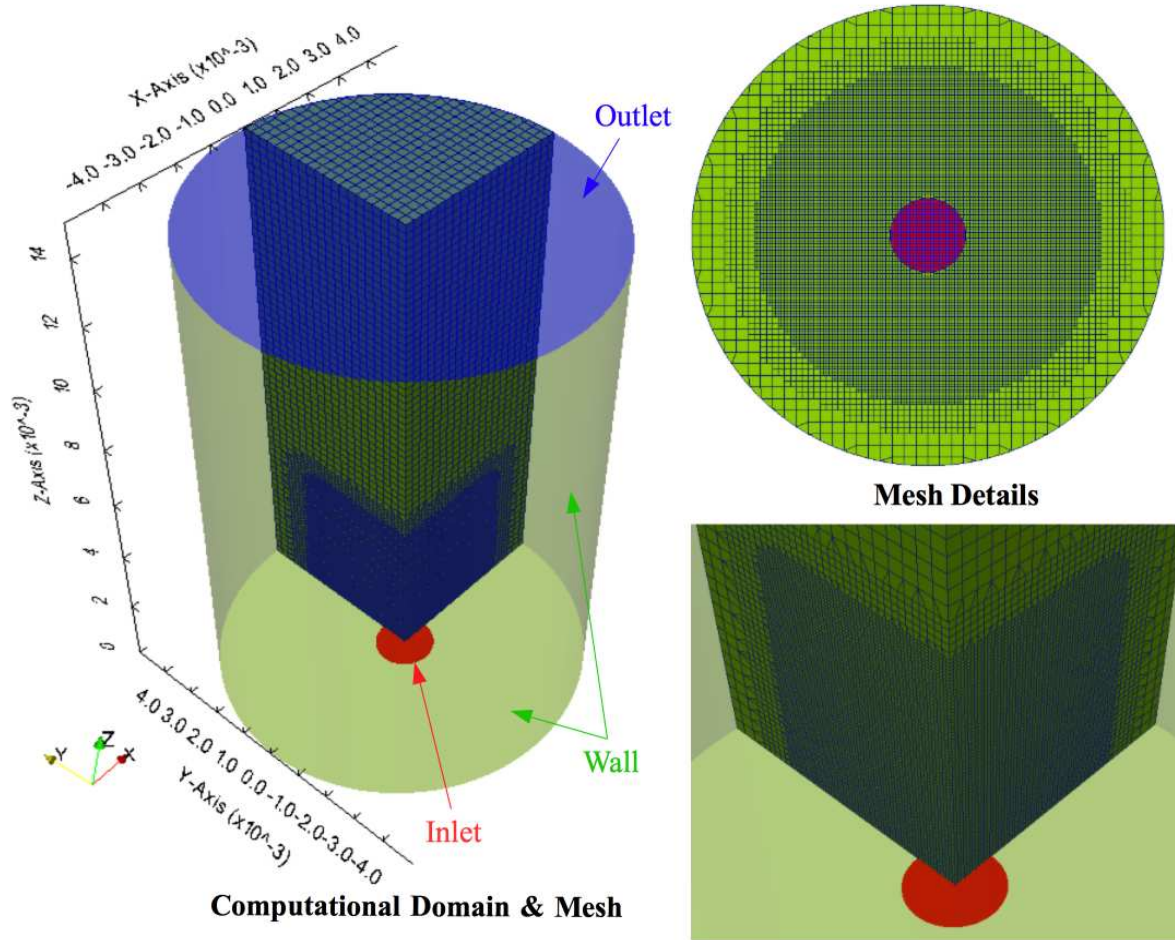


Fig. 14. Computational domain, mesh and boundary conditions.

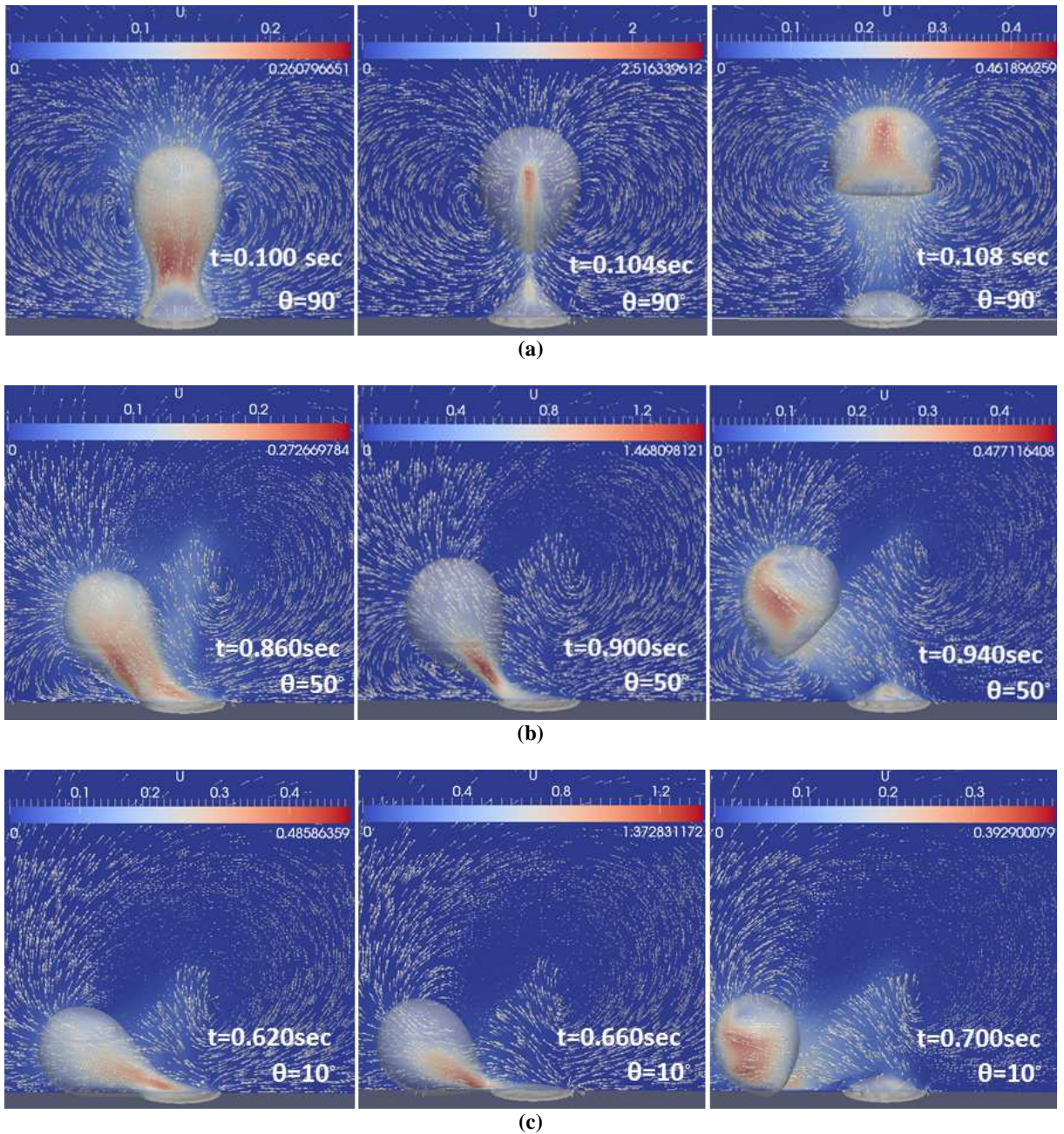
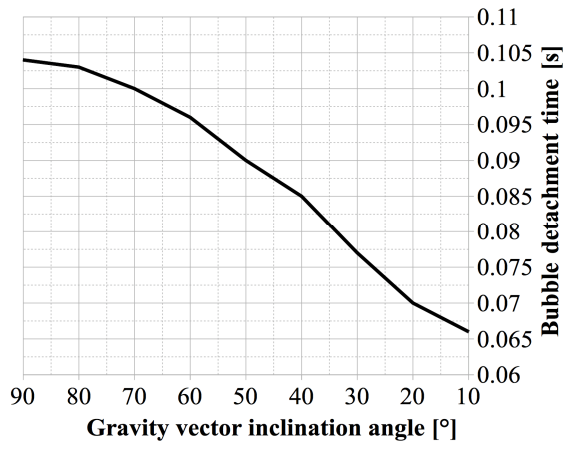
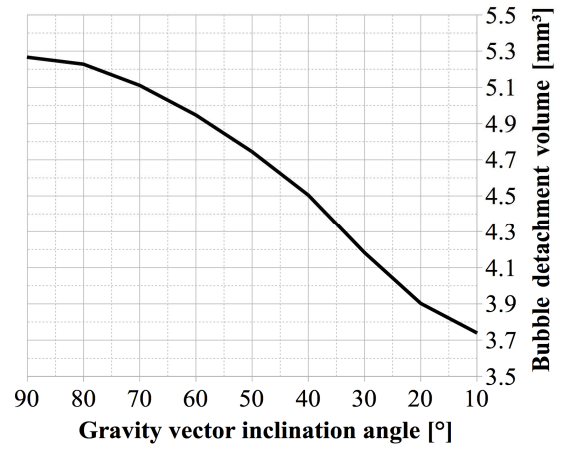


Fig. 15. Adiabatic bubble growth and detachment of R245fa vapour injected into a R245fa liquid, for different gravity vector inclinations with relation to the horizontal plane: $\theta=90^\circ$ (a), $\theta=50^\circ$ (b) and $\theta=10^\circ$ (c). For each inclination angle three different time instances are illustrated (the time of detachment and 4 msec before and after).



(a)



(b)

Fig. 16. Diagrams of (a) bubble detachment time and (b) bubble detachment volume, with respect to the gravity vector inclination angle.